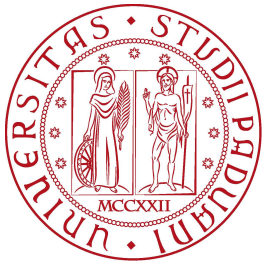

Università degli Studi di Padova

DIPARTIMENTO DI TECNICA E GESTIONE DEI SISTEMI INDUSTRIALI

CORSO DI LAUREA MAGISTRALE IN INGEGNERIA MECCATRONICA

TESI DI LAUREA MAGISTRALE

Combination of linear and nonlinear control of MSM based actuator

Relatore: Prof. Roberto Oboe
Correlatore: Prof. Michael Ruderman

Laureando: Matteo Sette
(matricola 2073386)

ANNO ACCADEMICO: 2024-25

This Master's thesis project was realised in collaboration with the University of Agder within the context of the Erasmus+ program. All experiments were conducted during the fall semester at the Grimstad campus, under the supervision of Professor Michael Ruderman.

First of all I want to thank Prof. Michael Ruderman for all the help and support that he gave me during this period. After that, I want to express all my gratitude to UiA for the organization and the effort to make this experience unforgettable. Among all of them, I want to thank Olav, a very kind guy with a endless love for helping people. After that, I would like to express all the joy and happiness that I lived during this unique experience. I met amazing people from a lot of countries and we spent some incredible moments here. I feel lucky for have met all of them and the minimum that I can do to thank them is to suggest everybody to try this experience. I think there is not any greater compliment to receive. Ci tengo poi a ringraziare i miei compagni di avventura italiani. Gianluca è stato un ottimo compagno di studio, di stanza e di avventura per questi 4 mesi. Voglio poi ringraziare Maria Elena, Davide e tutti i dottorandi che ci hanno fatto sentire un po' come a casa, auguro a tutti loro un futuro brillante. Qui voglio poi ringraziare anche tutto il personale della taverna Birdland, sono stati come una seconda famiglia per me, tra alti e bassi, abbiamo servito con il sorriso un pasto caldo a tutti. Un abbraccio forte và a tutti i miei amici, un gruppo disomogeneo e disorganizzato di ragazzi che, non si sa come, riescono ancora a tenere a galla una barca che mi scalda sempre il cuore. Ma più di tutti voglio dedicare questa esperienza alle due famiglie che sono fortunato di avere, Gabriella e Gianni, Nadia e Gabriele. Del loro supporto e del loro amore io e Fabio non saremo mai grati abbastanza. Infine tra queste pagine voglio ricordare Enzo, sarei stato felicissimo di rivederlo al mio ritorno. Dedico a lui tutti le serate bagorde di cui avrebbe sicuramente riso molto.

Grazie mille di cuore a tutti.

Matteo

Abstract

Since the advent of the new millennium, the scientific community has been engaged in the study of novel smart materials, with the objective of reaching new and higher levels of performance. Such interest is shared by industry, which is required to meet new technological challenges on a daily basis. From the field of surgery to the domain of competitive racing, the control of an object's position has been a subject of study for several years. However, with the advent of automated production lines, this need has become a fundamental requirement. One of these the new technology is Magnetic Shape Memory (MSM) was developed. However, this potential technology presents certain issues in terms of control, which have become a central focus of numerous researchers. In particular, the strongly nonlinear behaviour of this element, identified as hysteresis, represents a significant challenge in achieving this goal. The objective of this Master's thesis is to integrate the conventional theory of control systems with a novel technique that has the potential to address, or mitigate, these challenging issues present in numerous other physical systems.

Author: Matteo Sette
(matricola 2073386)

Contents

Chapter 1

Introduction

The main goal of this work, and of research in general, is to provide a useful contribution in order to achieve new and higher performance standards. To reach this objective, the study of new materials is crucial in the field of mechanical engineering, where precise and rapid control of motion is required. This research focuses on one such material class, known as 'smart actuators.' The use of these materials leads to simpler, lighter, and more reliable systems compared to conventional technologies such as hydraulic and pneumatic systems, while minimizing energy consumption, enhancing structural lifespan, and reducing maintenance costs. Achieving these results requires the development of new materials capable of producing large strokes under precise and rapid control. Currently, the most widely used technologies are:

1. *Piezoelectric materials*: These exhibit rapid response but produce small strokes when subjected to an electric field.

2. *Magnetostricitive actuators*: These undergo strain when a magnetic field is applied, causing the rotation of magnetic domains within the material. They offer rapid response, can generate forces 20 times greater than those produced by piezoelectric materials, and have an energy density 10 times higher than hydraulic systems. However, their strain is limited to approximately 0.17%.

3. *Shape Memory Alloys (SMA)*: When plastically deformed at one temperature, they can recover their original shape upon heating. These materials produce large strokes but have slow response times due to the thermal control process, especially during cooling.

To develop a material capable of producing large strains and high forces with rapid response times, Magnetically Controlled Shape Memory Alloys

(MSMAs) have been introduced. To explain how an MSM works, the behaviour of the SMA needs to be explained. These materials undergo an internal crystalline transformation from 'austenite' at high temperature to several variants of 'martensite', including multiple twins, during the cooling process. When the SMA is in the martensitic phase and a unidirectional stress σ is applied, a temperature dependent critical stress $\sigma(T)$ begins to detwine the martensitic phase leading to a single variant aligned with the axis of stress loading. A similar condition is achieved when the SMA starts in the austenitic phase. If T is significantly low during the phase transformation, a large residual strain remains after unloading and a significant apparent plastic deformation is achieved. This strain can be recovered by heating the SMA, this behaviour is called "shape memory effect". This process can be controlled by constraining the SMA so that partial recovery of strain is achieved, but some stress is present to prevent full recovery.

1.1 MSM: state of art

The actuation of these materials relies on controlling the shape memory effect through the reorientation of martensitic unit cells in an applied magnetic field. For the shape memory effect to occur, the martensite must exhibit a twinned substructure. In this configuration, the martensite variants with the easy magnetization axis aligned with the magnetic field increase their relative volume and dominate at the expense of other twins (see Fig.1.1).

More in detail, (a) MSM alloys have only variant 1 in the first state; (b) with the strong magnetic field applied in the y-direction, the MSM element stretches in the x-direction. The elongation stops when all twins switch to variant 2; (c) Under weak or no magnetic field, MSM magnetic field, MSM alloys can maintain their length; (d) MSM alloys can contract with the application of a magnetic field in the x-direction; (e) MSM alloys can contract with the application of a compression force. (f) MSM alloys can return to their original position by process (d) or (e). See articles [2, 3] for more details. The result is an actuator capable of achieving indicated strains of 4%-6% (the largest MSM effect in Ni-Mn-Ga alloys has been shown close to 10% [4]) with control that is both rapid and precise, within the milliseconds range. For this reason, they are considered promising candidates for active elements in compact electromagnetic actuators, sensors, generators, and dampers.

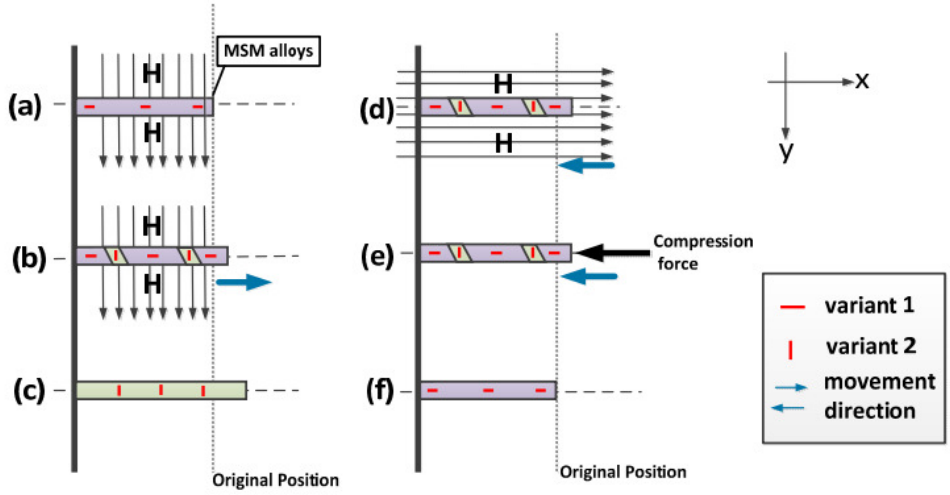

Figure 1.1: Presentation of the MSM effect in a single crystalline actuating element (source: [1]).

1.2 Previous works

Despite the good performance of the MSM-based actuator, the technology has not yet entered the market, although a large number of demonstrators have been presented for a variety of possible applications. One of the main technical reasons for this lack of commercialization seems to be the complexity of the design process of MSM-based actuator systems related to the non-linear and hysteretic magneto-mechanical coupling of MSM. A field-stress-strain MSM hysteresis is particularly inconvenient for under varying operating conditions such as temperature, frequency and non-constant mechanical loads. The hysteresis effect causes inaccurate positioning performance, e.g. if an actuator with hysteretic non-linearity is used in the closed-loop system, the hysteresis will cause unwanted oscillations and even instability. In order to compensate for the hysteretic behaviour, many modeling approaches have been implemented [5, 6, 7]. Much research has been carried out into control systems hysteresis between piezoelectric and magnetostrictive actuators. However, only a few studies have been devoted to the MSM specific control problems [8, 9, 10].

1.3 Contribution of this work

The main objective of this work is to implement a control strategy for the position control of a MSM-based actuator. In order to achieve this goal,

an identification algorithm of the hysteresis introduced by the actuator is implemented. The central point of interest of this part of the work is the study of a computationally efficient strategy that can be proposed for real-time application. Once the on-line identification of the non-linear behaviour of the actuator is achieved, the compensation of the hysteresis is implemented. The combination of feedforward and feedback control is analyzed to optimize the overall performance of the control system. In the present study, a Ni-Mn-Ga MSM element with dimensions of 20 mm x 3 mm x 1 mm, was employed (see Fig. 1.2).

Figure 1.2: MSM element (AdaptaMat, 2008).

Chapter 2

MSM actuator

In this first chapter, the MSM actuator is described and modeled in order to develop an appropriate position control loop. Furthermore, a computationally efficient technique for hysteresis modeling is analyzed, with the simulation results presented.

2.1 Linear and non linear behaviour

A MSM element constitutes an intrinsic transducer which converts the fed magnetic energy into the twin-boundary motion. It's also possible to achieve the same effect applying an external mechanical stress to the material in order to describe the total stress applied to the element σ:

$$\sigma(\varepsilon) = \sigma_{ext} + \sigma_{mag}(h_e) \tag{2.1}$$

Where σ_{ext} is the external mechanical stress applied to the material and σ_{mag} is the stress produced by the applied magnetic field h_e. Some experiment demonstrated that the strain ε exhibits an hysteretic behaviour that can be described with the equation:

$$\varepsilon = \Gamma^{-1}(\sigma_{ext} + \sigma_{mag}(h_e)) \tag{2.2}$$

Where Γ is an hysteresis map. This means that energy dissipation occurs at each conversion stage and the principal cause is due to the work required for a lattice reorientation during the twin boundary motion. In addition, it's important to keep in mind the presence of eddy currents, hysteresis losses in iron core of the magnetizing system, flux leakage losses in the air-gap, as well as the frictional and structural losses in the mechanical drive. So the MSM strain constitutes the dynamic input nonlinearity

and represents a structural rearrangement of a large number of martensite twin variants. For this reason, the Preisach-type hysteresis model appears as particular suitable for a MSM modeling considering that the superposition of multiple elementary hysteresis operators (referred as 'hysterons' $\gamma_{\alpha\beta}$) is high analogously to the mechanisms acting on the twin variants. To describe the MSM strain in function of the applied external magnetic field and mechanical stress, it is possible to use the following expression:

$$\varepsilon(t) = \iint_P \rho(\alpha,\beta)\gamma_{\alpha\beta}[\chi[h_e(t),\sigma_{ext}(t)]]\ d\alpha d\beta \tag{2.3}$$

Where P is the Preisach plane where the density function $\rho(\alpha,\beta)$ is defined and the operator χ transfers both hysteresis inputs into a mechanical internal stress.
To identify the linear behaviour of the actuator is necessary to describe its structure. The MSM element is housed inside a black box, where a screwed spring is used to return the element to its original position when the magnetic field is no longer applied (see Fig.2.1).

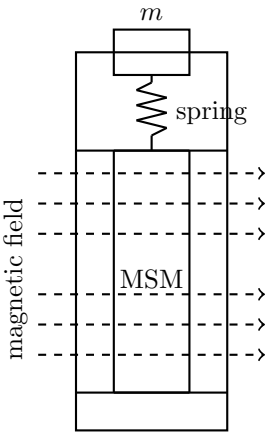

Figure 2.1: Structure of the actuator.

It is important to emphasize that the calibration process of the spring is crucial to achieving optimal results. In particular, if the spring exerts too much force on the MSM element, a shorter displacement can be observed, while if the spring is not screwed tightly enough, it will result in a non-zero position when the MSM is not excited. The dynamic MSM actuator model of this structure can be describe using a spring-mass-damper system (see fig.2.2) where:

The concentrated mass m includes the mass of the MSM element, output push rod, and mechanical interface between both.

Stiffness k represents the return spring connected with the moving mass.

Damping element d represents an aggregated viscous damping of the bearing and structural damping of the spring.

Force Fp is the pre-stress applied to all elements within the fixed mounting frame in direction of the relative displacement.

The expense of the gravity acting due to the vertically moving mass is quite low in comparison to the output force, so that the gravity impact is fully neglected during the modeling.

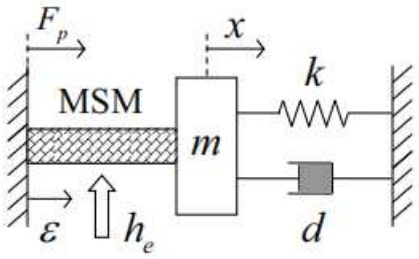

Figure 2.2: Dynamic actuator model when the MSM element is excited by a magnetic field (source:[11]).

The pre-stressed actuator dynamics is:

$$m\ddot{x} + d\dot{x} + k(x - \varepsilon) = F_P \tag{2.4}$$

Where $F_P = A\sigma_{ext} = k(x - \varepsilon)$ in static-condition with $\varepsilon = f(h_e, \sigma)$. The eigen behavior and nonlinearities of the applied magnetization system are omitted from consideration, due to a strong coupling with the MSM behavior and the lack of measurability. This simplification assumes that the active MSM element closes the magnetic circuit without changing significantly the magnetic flux in the air gap during the elongation . Since no field measurement and control are available, from a closed system point of view the controllable coil current constitutes the input value and the induced relative displacement constitutes the output value of the MSM based actuator. From eq.2.4 it is evident that the output relative displacement is lagged behind the applied input force due to the second order actuator

dynamics. At the same time, the hysteresis nonlinearity constitutes the rate-independent map so that no frequency dependent lag occurs (see an example in fig2.3).

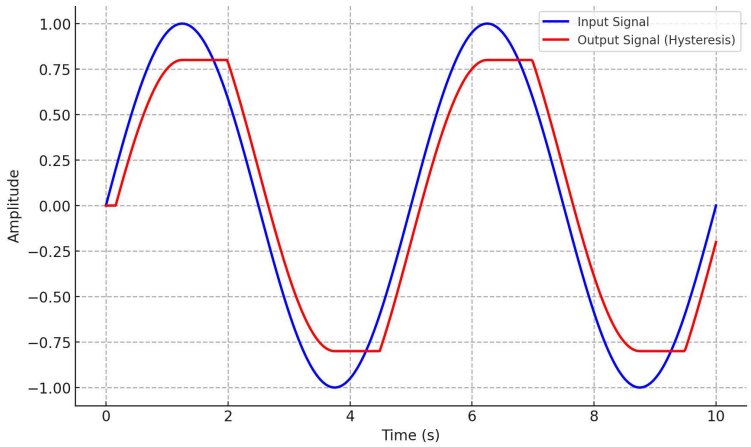

Figure 2.3: Time evolution of hysteresis phenomena.

A frequency analysis on the spectrum [0 300]Hz reveals the following behaviour:

$$G(s) = \frac{45.57}{s^2 + 737.9s + 5.439e05} \exp(-0.002s) \tag{2.5}$$

Where the variable s is the Laplace variable used for frequency-domain representation of linear time-invariant systems. It's interesting to notice that the frequency-independent input lag is attributed to the hysteresis. From the eq.2.5 is possible to get the natural angular frequency $w_n = 737$ rad/sec and the damping factor $\xi = 0.5$ Knowing these parameters and the moving-mass $m = 0.0015$ kg, to find the physical parameters of stiffness k e damping d is simple.

$$\begin{cases} \omega_n = \sqrt{\frac{k}{m}} \;\rightarrow\; \text{k} = 815.7835\ N/m \\ \xi = \frac{d}{2\sqrt{mk}} \;\rightarrow\; \text{d} = 1.1069\ Ns/m \end{cases} \tag{2.6}$$

To validate the model a comparison between the real step response and the modeled one is reported in fig.2.4.

Finally the bode plot of the eq.2.5 is reported in fig.2.5.

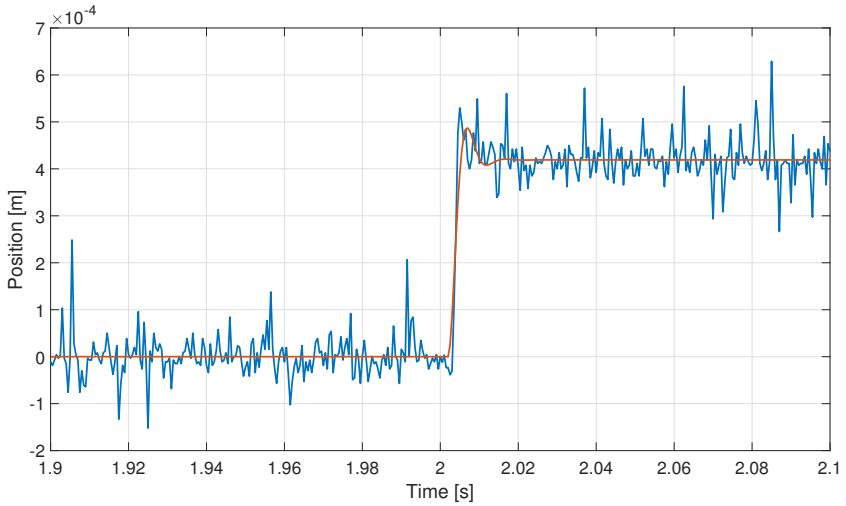

Figure 2.4: Measured and computed step response comparison.

2.2 Hysteresis modeling

The phenomenon of hysteresis is encountered in many areas of science but the large amount of interpretations is a result of the need of a rigorous mathematical definition in order to avoid confusion and ambiguity. The scalar Preisach hysteresis model is a universal mean for describing the rate-independent phenomena that remains a widely accepted and reasonable approach for describing this behaviour in functional materials. This model was based on some assumption concerning the physical mechanism of magnetization but later this tool evolved in a pure mathematical form separated from its physical meaning. This formulation cannot represent every hysteresis nonlinearities but some essential conditions have to be satisfied:

- The output y depends on the sequence of input values but not on the frequency with which they are proceeded. As originated from an ancient greek word "hysteresis", meaning "lagging behind", this effect is mathematically described as a negative-signed integral of the phase shift over a full period, in every scenario.

- The past exerts its influence upon the future through instantaneous values of output.

- Any past history can be wiped out by input oscillations of sufficient large magnitude. This is called 'wiping-out property' and was proved

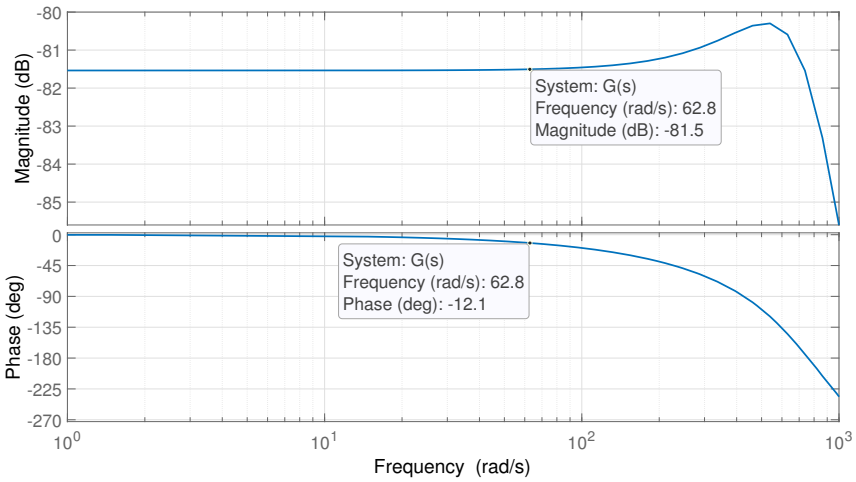

Figure 2.5: Bode plot of the G(s) transfer function.

by several experiments in the area of magnetics that showed the evidence of major hysteresis loops whose shapes don't depend in how they are approached.

- All hysteresis loops corresponding to the same extreme values of inputs are congruents, i.e. they have the same shapes.

Once these conditions are satisfied, the Preisach model can be used as described in this section. Consider a infinite set of simplest hysteresis operators $\gamma_{\alpha\beta}$. These operators represent rectangular loops on the input-output plane (see fig.2.6) where α and β correspond to 'up' and 'down' switching values of input. The output of these operators can assume ± 1 only.

The hysteron's states is given by:

$$\gamma_{\alpha\beta}(t) = \begin{cases} -1, & \text{if } x(t) \leq \beta \\ +1, & \text{if } x(t) \geq \alpha \\ y(t_0), & \text{if } \beta < x(\tau) < \alpha \ \ \forall\, \tau \in [t_0, t] \end{cases} \tag{2.7}$$

Where the switching threshold values (α, β) define the position of the hysterons on the Preisach half-plane $\alpha \geq \beta$. The classical model formulation is given by:

$$f(t) = \iint_{\alpha \geq \beta} \mu(\alpha, \beta) \gamma_{\alpha\beta} x(t)\, d\alpha d\beta \tag{2.8}$$

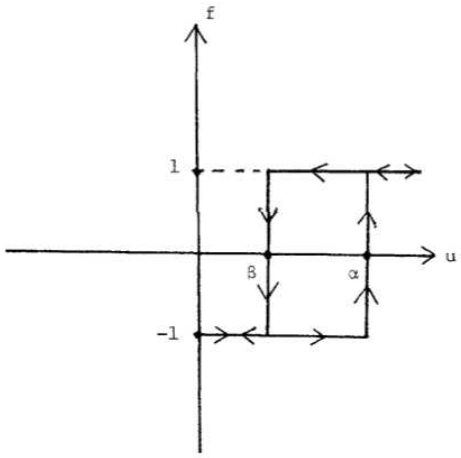

Figure 2.6: Hysteresis modeling. Elementary hysteron operator $\gamma_{\alpha\beta}$ (source:[12]).

Where $\mu(\alpha, \beta)$ entirely parameterize the Preisach hysteresis operator. The study of eq.2.8 can be facilitated dividing the Preisach plane in 2 areas: P^+ consisting of the points where $\gamma_{\alpha\beta} = +1$ and P^- where $\gamma_{\alpha\beta} = -1$. Using this geometrical interpretation the model can also be represented with the following form:

$$f(t) = \iint_{P^+(t)} \mu(\alpha, \beta)\, d\alpha d\beta \; - \iint_{P^-(t)} \mu(\alpha, \beta)\, d\alpha d\beta \tag{2.9}$$

For practical utilizes an infinite number of hysterons is not realizable. For this reason it's necessary to discrete the Preisach half-plane in L = $(N^2+N)/2$ parts where N is called 'discretization level of the Preisach plane'. In this way the discrete Preisach hysteresis model can be seen as the superposition of a finite number of hysteron whose contribute on the total output is given by:

$$y(t) = \sum_{i=1}^{L} \mu_i \gamma_i(x(t), y_i(t_0), \alpha_i, \beta_i) \tag{2.10}$$

In this particular work the input signal is included in the range [0 5] A, for this reason a equally spacial distribution of hysterons is reported in fig.2.7 (for more details about the software implementation, see Appendix A.1).

The aim of this part of work is to introduce a new computationally efficient formulation of a Preisach hysteron with a low set of primitive

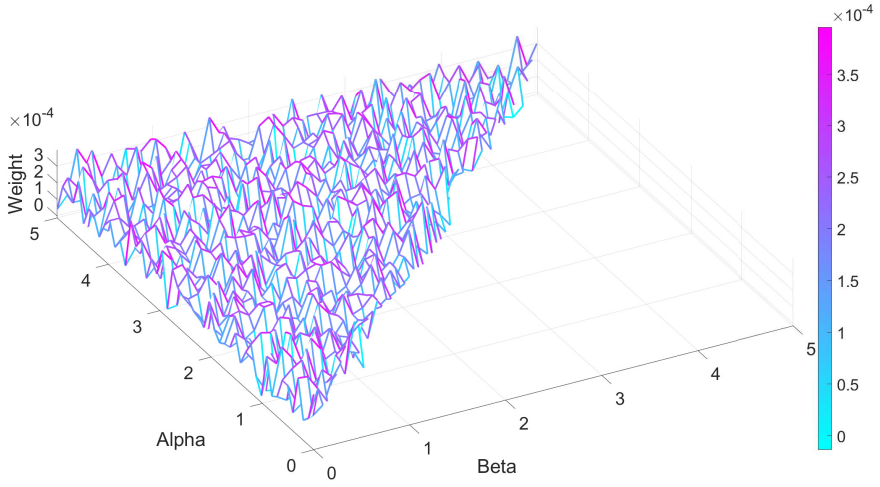

Figure 2.7: Hysteresis modeling. Random density function whose sum of all the weights is unitary.

operations required: two summation, two sign operators, two comparison and one memory storage for the previous stage. The algorithm is described in fig.2.8.

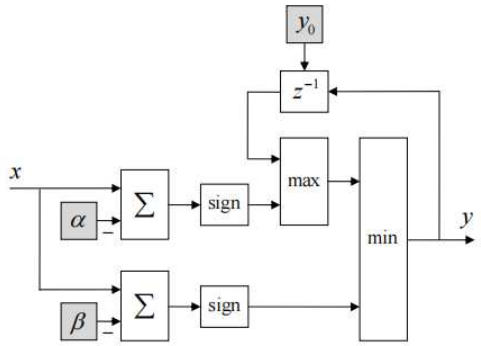

Figure 2.8: Hysteresis modeling. Blocks scheme of an elementary hysteron (source:[13]).

To describe the algorithm we refer to the fig.2.6 where is possible to observe that the eq.2.11 well describe the behaviour when $x(t) \leq \beta$ or $x(t) \geq \alpha$.

$$\min[\text{sign}(x-\beta), \text{sign}(x-\alpha)] \tag{2.11}$$

Considering now the interval $x(t) \in (\beta, \infty)$ and the switching condition

sign(x-α), it's possible to describe the behaviour in this working area as:

$$\max[\text{sign}(x-\alpha), y(t_-)] \tag{2.12}$$

Where $y(t_-)$ is the previous state and, in case of initial state, it assumes the value:

$$y(t_0) = \begin{cases} \text{sign}(x(t_0)), & \text{if } x(t_0) < \beta \text{ or } x(t_0) > \alpha \\ [-1,+1], & \text{otherwise}. \end{cases} \tag{2.13}$$

Combining the eq.2.11 and eq.2.12 the entire behaviour of a single hysteron can be described as following:

$$y(t) = \min[\text{sign}(x-\beta), \max(\text{sign}(x-\alpha), y(t_-))] \tag{2.14}$$

2.3 Numerical simulations

The algorithm is tested in real time to prove the effective parallel processing of the system (for implementation details see ChapterA). The goal of these simulations is to evaluate the highest performance of the algorithm with a sampling rate of 2 KHz. The first test is made using a Preisach plane subdivided in 20x20 parts for a total of 210 hysterons. The results are reported in fig.2.9.

In particular one of these experiment (Fig.2.9c) demonstrate the property of congruence described before. In Fig.2.9d it's possible to observe some internal hysteresis generated by sinusoidal inputs of low amplitude. Most of them are completely hidden from the external loop hysteresis that wipe-out the state of the minor ones (wiping-out property).

In fig.2.10 is possible to appreciate the effect of the discretization of the Preisach half-plane. This comparison highlights a more rough characterization of the hysteresis operator for $N \leq 30$. The advantage of a high-resolution of the Preisach plane is limited from the real time processing of the algorithm, to process an higher number of hysterons is necessary to reduce the sampling time.

Another interesting test is to observe the effect of two different Preisach density $\mu(\alpha, \beta)$, represented in fig.2.11, on the hysteresis model (see fig.2.12). This behaviour is explained using the geometrical interpretation, where $\mu(\alpha, \beta)$ express how much the hysteresis is affected by the input into that precise zone of the Preisach plane. This consideration indicates that the density function affects the shape of the hysteresis model, representing another parameter to take into account during the projecting phase.

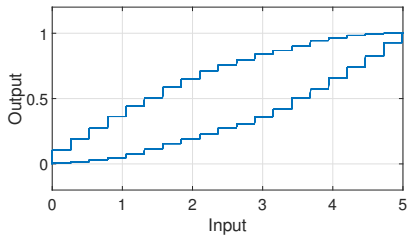

(a) Response to a sinusoidal input,

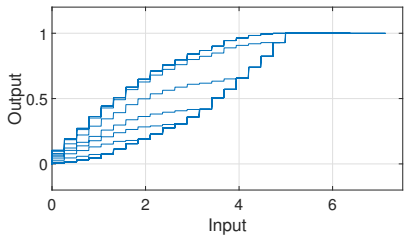

(b) Response to a increasing sinusoidal input,

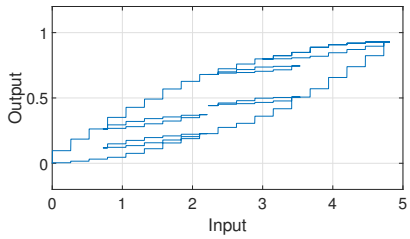

(c) Response to a product of sinusoidal inputs,

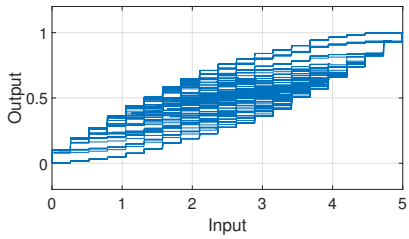

(d) Response to a sinusoidal signal with random amplitude,

Figure 2.9: Hysteresis numerical simulation. Response to different inputs by a hysteresis computed with 210 elementary hysterons.

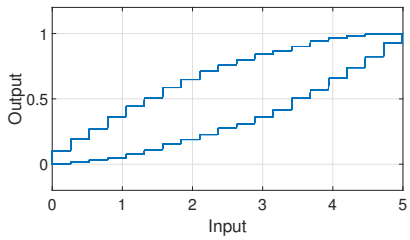

(a) Mesh 20x20, L = 210

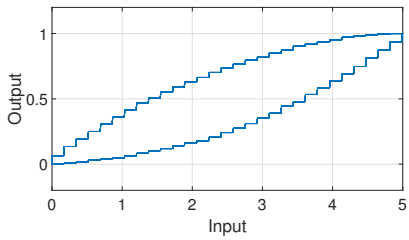

(b) Mesh 30x30, L = 465

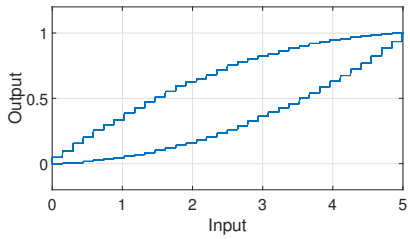

(c) Mesh 35x35, L = 630

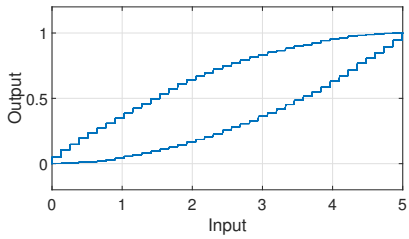

(d) Mesh 40x40, L = 820

Figure 2.10: Hysteresis numerical simulation. Effect of different resolutions of the Preisach plane.

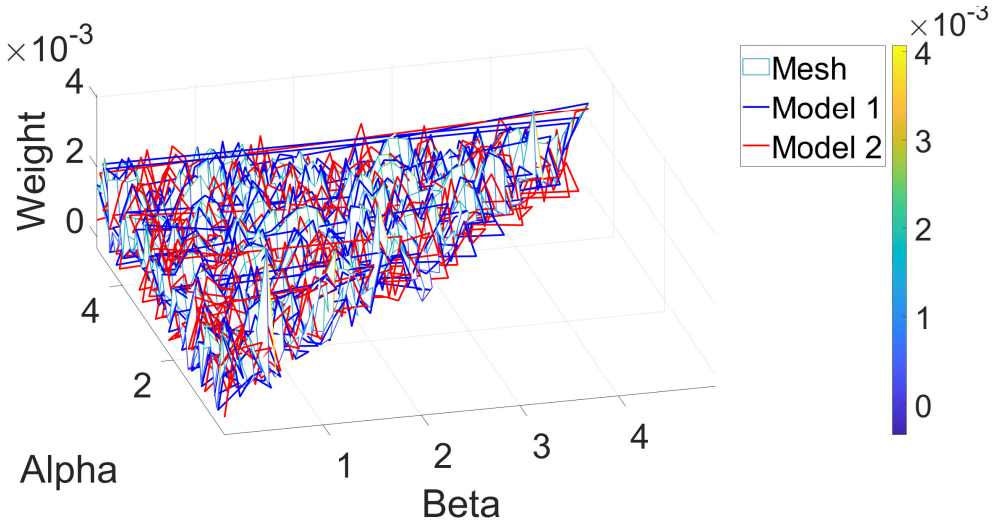

Figure 2.11: Hysteresis numerical simulation. Different normalized density function $\mu(\alpha, \beta)$ on the Preisach plane.

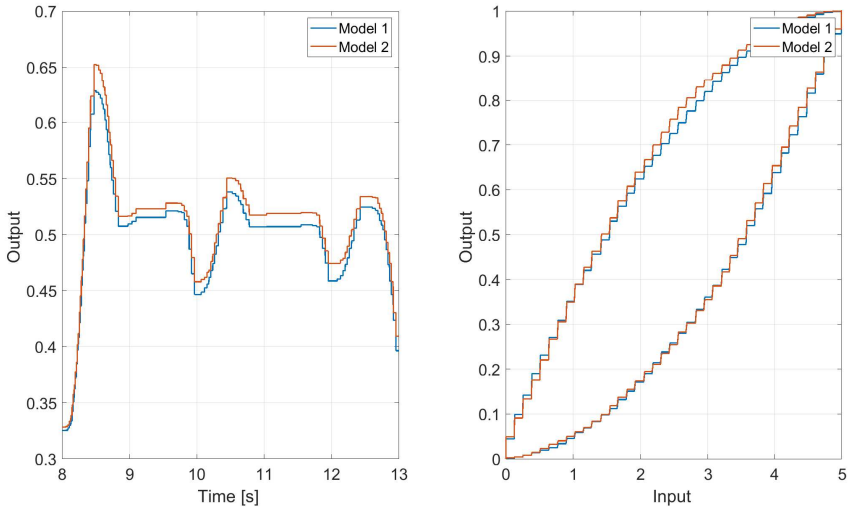

Figure 2.12: Hysteresis numerical simulation. Effect of different density functions $\mu(\alpha,\beta)$ on the output model (left) and on the shape of the hysteresis model (right).

In conclusion, the algorithm reproduces correctly the hysteresis phenomena without any violation on the necessary conditions to apply the Preisach model. A computational limit is reached in real-time condition using a sampling rate of 2 KHz on a 35 x 35 mesh equivalent to L = 630.

Chapter 3

Control approach

In this chapter, the experimental setup (Fig.3.1) is illustrated to explain how to practically achieve the goal of controlling the position of the actuator. Moreover, the control system plant is explained and analyzed in order to describe the process of tuning of the regulator.

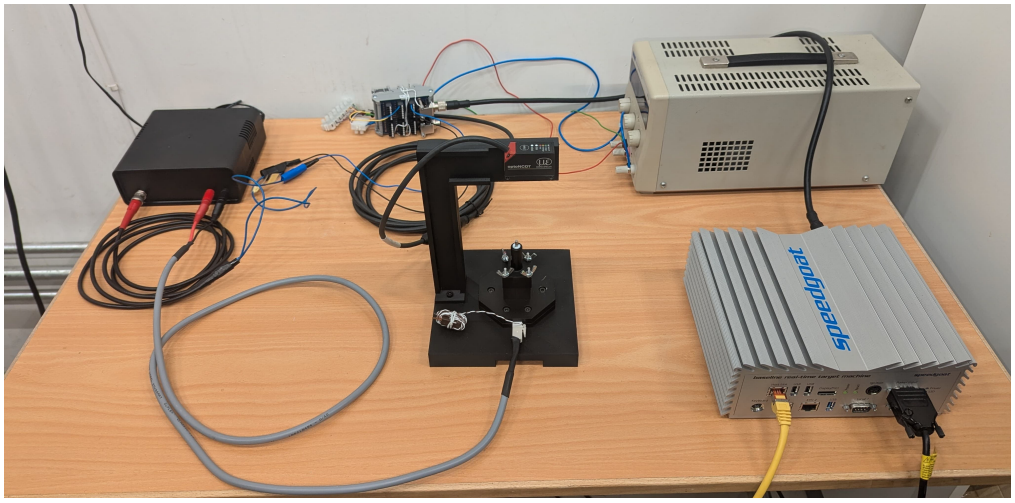

Figure 3.1: Experimental setup (UiA mechatronics laboratory view).

3.1 System plant

The MSM-based actuator is produced by 'Adaptive Materials Technology' and provides a DC connection to the excitation coils that can produce a field strength of about 400−500 kA/m, required to produce the maximum strain of the MSM element. The nominal characteristics of the MSM

Main features	Value
Strain or stroke	typically 3-5 %
Force density	1-2 MPa
Work output (force x stroke)	max 100 kJ/m^3
Operating frequency	up to 1-2 KHz
Operating temperature	max 40 °C

Table 3.1: MSM datasheet provided by the manufacturer.

element are reported in table3.1.

It is important to emphasize that the calibration process of the spring is crucial to achieving optimal results. In particular, if the spring exerts too much force on the MSM element, a shorter displacement can be observed, while if the spring is not screwed tightly enough, it will result in a non-zero position when the MSM is not excited. Moreover, in order to reach a deterministic (further as 'accommodated') response to a homogeneous periodic excitation, the actuator has to leave first the memorized initial state, that will be called a 'transfer' response. From the experiment (see fig.3.2) it's evident that the transfer response crosses two different transitions before reaching the level of accommodated response which remains nearly constant during the remaining execution time. Note that the remarkable diversity between the transfer and accommodated response cannot be attributed to the warm-up of the MSM actuator.

The laser displacement sensor is called optoNCDT ILD 1420-200 and is produced by 'Micro-Epsilon'. It is integrated in a small case of 20 x 30 x 46 mm size and it provides an integrated cable 0,3m long with 12 pin connector. The most relevant information about this sensor are reported in the table3.2.

To connect the sensor to the digital controller, a current-to-voltage con-

Main features	Value
Measuring range	200mm (from 60 mm to 260 mm)
adjustable measuring rates	4 kHz/2 kHz/1 kHz/0.5 kHz/0.25 kHz
Repeatability	8 μm at 2 KHz
Analogue output	from 4 mA to 20mA
Power supply	from 11 VDC to 30VDC

Table 3.2: Laser sensor's main characteristics provided by Micro-Epsilon.

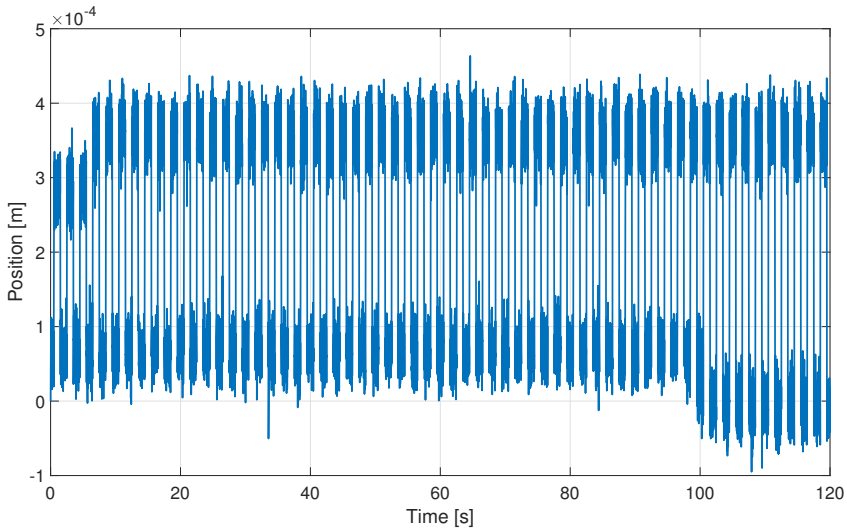

Figure 3.2: Initialization process using a train pulse input.

version is necessary. For this purpose, the PCF1402-3/U interconnecting cable is used to convert the current produced by the sensor into a voltage within the range [1V... 5V]. The power supply for the laser sensor is provided by the EX355, manufactured by AIM-TTI INSTRUMENTS. The sensor is fixed above the actuator using a structure designed with SolidWorks software and 3D-printed to ensure that the sensor remains stable and unaffected by the vibrations produced by the MSM element. The digital controller is SpeedGoat RealTime Target, which is connected to the computer using an Ethernet cable. It is used to execute the control strategy, to collect and filter the data received from the sensor, using the software Matlab/Simulink 2019b. Specifically, to remove noise from the signal, a digital second order low-pass filter is applied. Its transfer function is:

$$F(s) = \frac{1}{(1 + s\tau_g)^2} \tag{3.1}$$

Where $\tau_g = 1/\omega_g$ is the time-constant of the filter and ω_g is the cut-off angular frequency of the filter corresponding to 10 Hz. The Bode plot is reported in fig.3.3.

Finally, a current control interface connects the SpeedGoat to the actuator to prevent overcurrents and deviations from the imposed current reference.

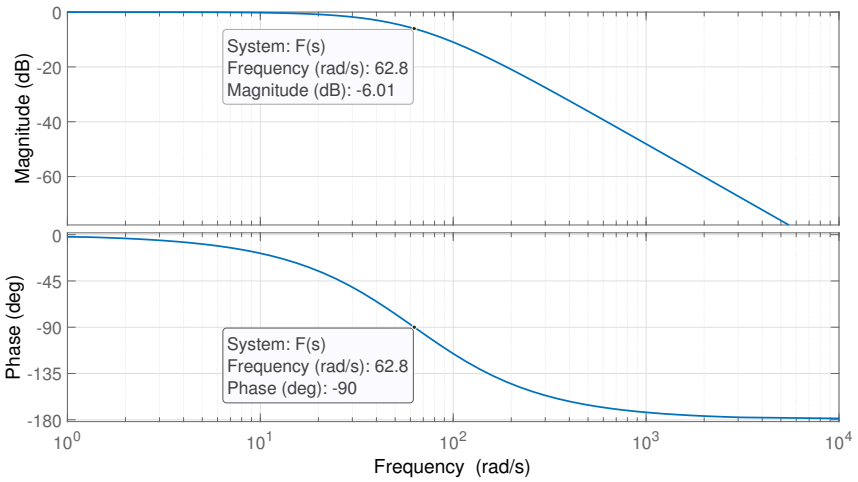

Figure 3.3: Bode plot of the second order low-pass filter $F(s)$.

3.2 Feedback control design

One of the most used feedback control regulator in industry is the Proportional Integral (PI) controller-based approach. This regulator grants an infinite gain at low frequencies reducing to zero the control error. On the other hand, it introduces a negative phase into the system leading to the instability if not well-tuned. A wide-used way to tune this type of regulators is the Bode synthesis. To apply this method, it is necessary to consider the function $L(s) = R(s)G(s)F(s)$, referred to as the 'Open-loop transfer function of the system', where:

- $R(s) = k_P + \frac{k_I}{s}$ is the transfer function of the regulator. In alternative a PID controller can be used introducing a derivative factor to obtain greater gain at high frequency with the disadvantage of amplifying the high-frequency noise;

- $G(s)$ is the transfer function of the process to control reported in eq.2.5.

- $F(s)$ is the transfer function of the low-pass filter (eq.3.1).

Given all the equations, except for $R(s)$, the only parameters to tune are k_P and k_I. Therefore, to solve the problem, it is necessary to find the solution to the following equations:

$$\begin{cases} |L(j\omega_a)| = 1 \\ \pi + \angle L(j\omega_a) = \varphi_m \end{cases} \tag{3.2}$$

Where ω_a is referred to as the 'control bandwidth' and representing the speed of the controlled system, while φ_m is called 'phase margin', which represents a measure of the stability of the system. In order to obtain a stable control system despite inaccuracies and noise affecting the control loop, a phase margin $\varphi_m = 1.4\ rad$ (equivalent to 80 degrees) is chosen. To define the project parameter ω_a the effect of the filter must be taken into account. Considering the cut-off frequency of this element $\omega_g = 10\ Hz$, the condition $\omega_a < \omega_g$ must be satisfied due to the attenuation effect of the filter at high frequencies. This constraint has to be considered with the stability limit, represented in fig.3.4, which shows the phase plot of the system actuator+filter having a total phase of -102 degrees. This makes clear that using a PI regulator at 10 Hz is not possible without violating the condition $\varphi_m = 80$ degrees considering that the PI regulator can introduce only negative phase.

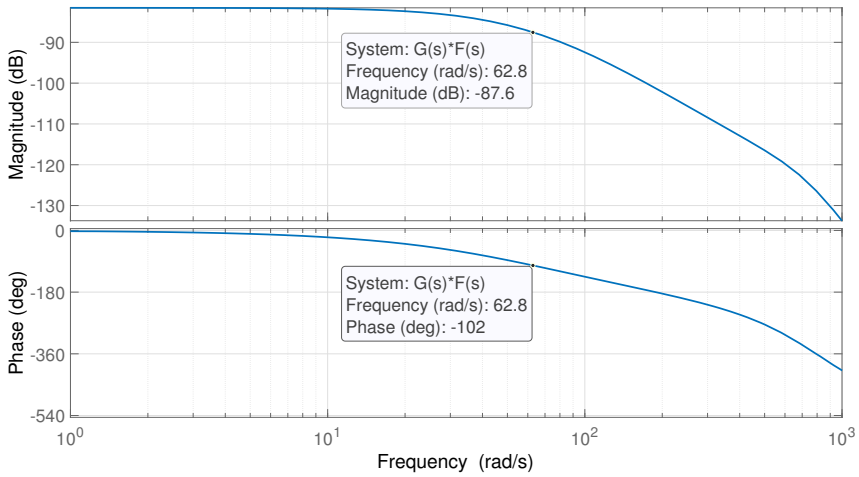

Figure 3.4: Feedback design. Bode plot of the system $G(s)F(s)$.

To achieve a phase margin of 80 degree, a total phase of the system equal to -100 degree is necessary. In order to reach this condition, it's necessary to operate below 62.8 rad/s. For tuning the regulator, a control bandwidth $\omega_a = 31.4$ rad/s (5 Hz) is chosen. At this frequency, the filter introduces a phase lag of 53 degree, while the system contributes a negative phase of 6 degree. The total effect results in a delay of -59 degree. Solving the system in eq.3.2 produces the following transfer function:

$$R(s) = 11279 + \frac{306138}{s} \tag{3.3}$$

The Bode diagram of this transfer function is shown in fig.3.5.

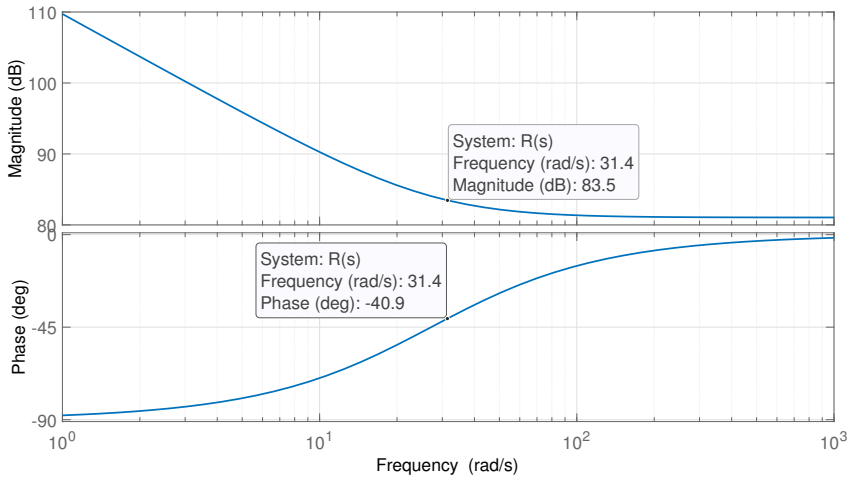

Figure 3.5: Feedback design. Bode plot of the PI regulator $R(s)$.

As shown in Fig.3.5, the regulator introduces a negative phase of 41 degrees, which is used to achieve the required -100 degrees of phase lag in the open-loop transfer function $L(s)$. To better understand the behavior of the entire system, the Bode plot of the closed-loop transfer function $Z(s) = \frac{R(s)G(s)}{1+L(s)}$ is provided here.

From Fig.3.6, it can be observed that the regulator is well-designed, and the closed-loop transfer function is stable with a sufficient phase margin.

3.3 Hysteresis nonlinearities compensation

To achieve better results in terms of control performances on the actuator, the nonlinear behavior of the MSM element is compensated using a non-classical approach. Specifically, an inversion-free feedforward compensation technique, as proposed in [14], is adopted in this work.

As well known, a feedforward stage always offers advantages in terms of performances because it operates independently of the signal produced by the measurement process, which is often affected by noise or low accuracy. This control strategy is valid if an accurate model of the system is presented considering that the feedforward control strategy is based on the inversion of the transfer function of the system to control (see fig.3.7).

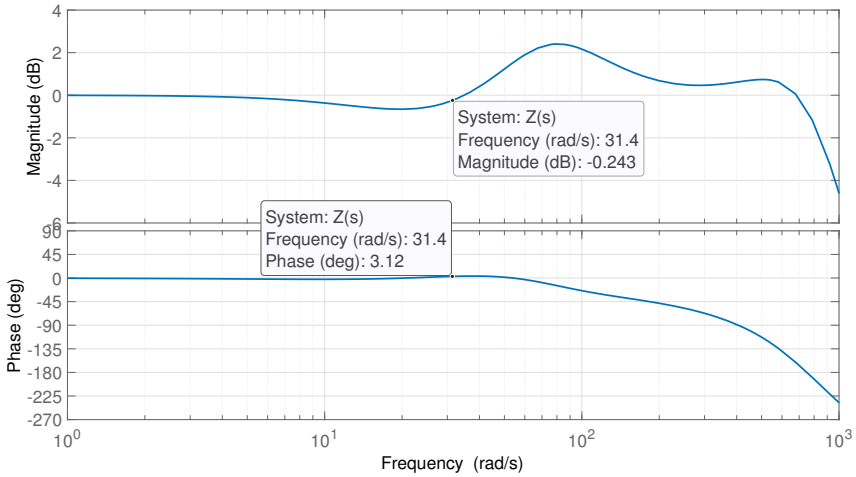

Figure 3.6: Feedback design. Bode plot of the closed loop Z(s).

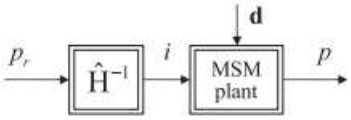

Figure 3.7: Hysteresis compensation. Scheme diagram of a feedforward control strategy (source:[10]).

Since this assumption is never valid, every control loop uses an auxiliary external loop of feedback to compensate the effect of external disturbance and inaccuracies on the model. The interaction between this two control methods is illustrated in Fig.3.8.

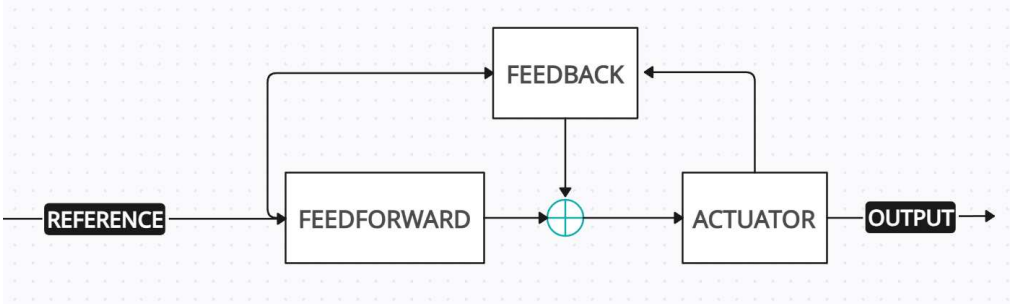

Figure 3.8: Hysteresis compensation. Total control system block diagram.

To define the feedforward block, a thorough understanding of the actuator is necessary. As described in Chapter2.1 1, the MSM element exhibits

a hysteretic behavior whose inverse cannot be directly obtained. The proposed feedforward control is based on the internal model principle and consists of a high-gain integral feedback loop that regulates the identified hysteresis model, as shown in Fig.3.9.

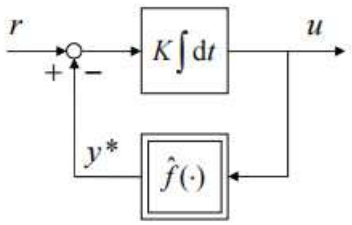

Figure 3.9: Hysteresis compensation. Inversion-free control loop (source:[14]).

If the control loop is well-designed, the modeled hysteresis should produce an output equivalent to the reference signal only when the desired input u is applied. The control law is:

$$u(t) = K \int (r(t) - y^*(t))\, dt \tag{3.4}$$

This loop mimics the inverse of the hysteresis function. To prove it, the result of the simulation with K = 1e07 is attached in fig.3.10.

Another interesting analysis to do is to observe the feedforward output in relation with the reference signal. Furthermore, to evaluate the performances of the system a plot reference-output is reported in fig.3.11 .

In Fig.3.11a is possible to observe the hysteresis used to feed the system to control. In Fig.3.11b the relation reference-output is similar to the desired linear ramp with unitary scope. Finally the time-evolution of the controlled system is reported in Fig.3.12.

A more detailed analysis of the sensitivity function $B(jw)$, where j is the imaginary unit and w is the angular frequency, is now reported to better understand the theoretical performances of this system.

$$B(jw) = \frac{e(jw)}{r(jw)} = \frac{r(jw) - y^*(jw)}{r(jw)} \tag{3.5}$$

where $y^*(jw) = Au(jw)$ is a rate-independent linear operator that describes the hysteresis behavior. Considering the entire feedforward system, the estimated output can be described as:

$$y^*(jw) = A\, \frac{K}{jw}\, e = A\, \frac{K}{jw} \frac{1}{1 + \frac{KA}{jw}}\, r(jw) \tag{3.6}$$

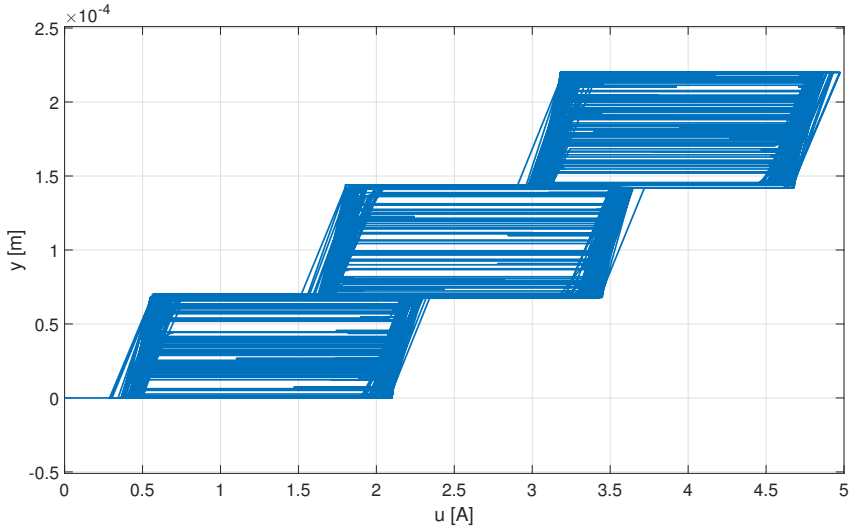

(a) Hysteresis to invert.

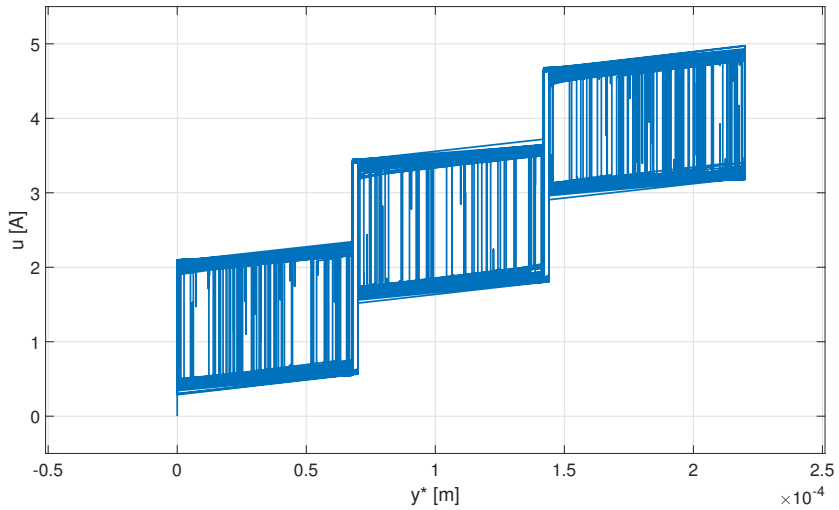

(b) Result of the inversion.

Figure 3.10: Hysteresis compensation. Result of the inversion of the hysteresis.

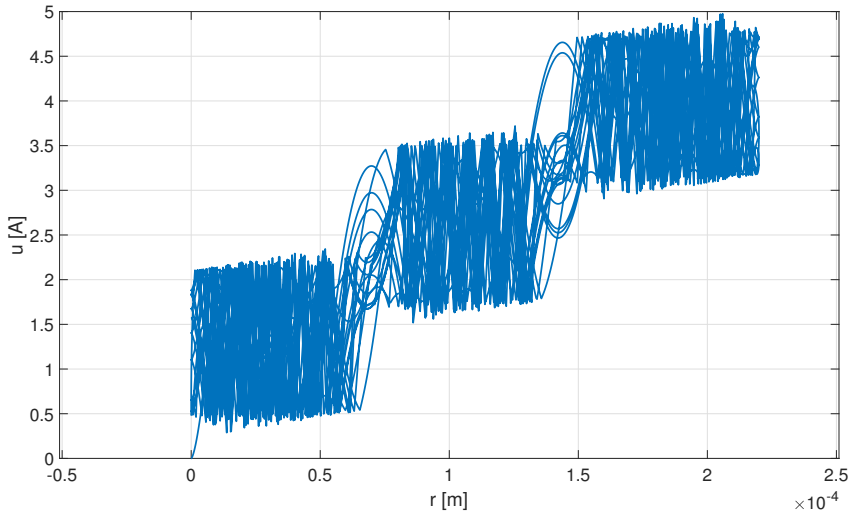

(a) Feedforward output generation.,

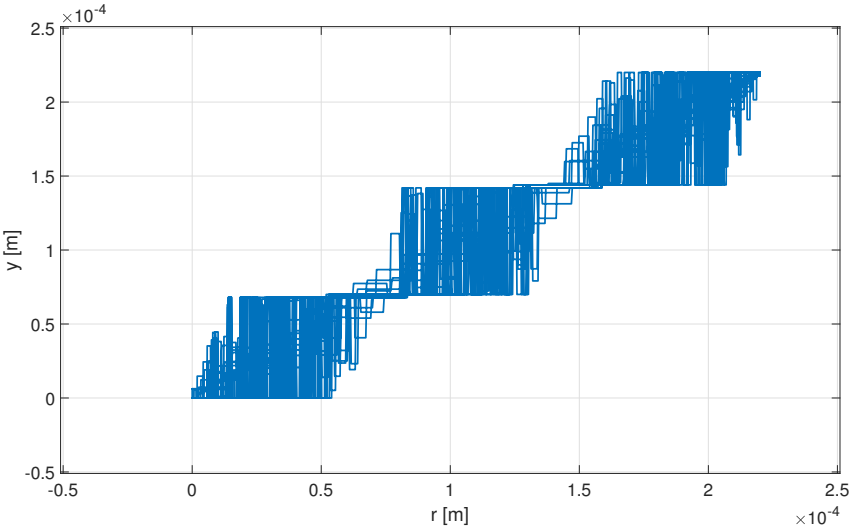

(b) Feedforward validation.,

Figure 3.11: Hysteresis compensation. Deeper analysis of the internal behaviour of the inversion process.

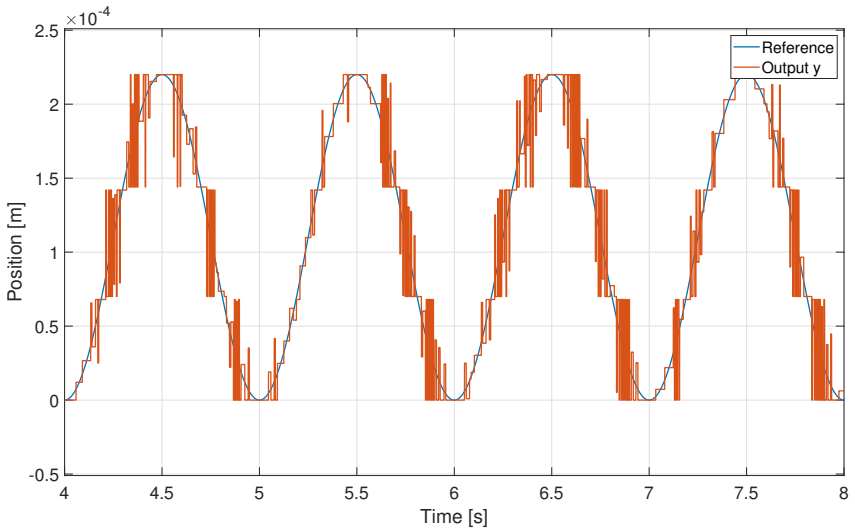

Figure 3.12: Hysteresis compensation. Behaviour of the system when controlled with only the feedforward technique.

The final equivalence in eq.3.6 can be obtained by recalling the relation valid for any closed-loop system: $\frac{y(s)}{x(s)} = \frac{A}{1+AB}$ where $y(s)$ in output, $x(s)$ is input, A is the open-loop transfer function and B is the process in feedback. From eq.3.6, it is possible to express the error as a function of the reference:

$$e(jw) = \frac{1}{1 + \frac{KA}{jw}}\, r(jw) \tag{3.7}$$

Substituting the eq.3.7 in eq.3.5 is possible to obtain the final expression:

$$B(jw) = \frac{e(jw)}{r(jw)} = \frac{1}{1 + \frac{KA}{jw}} = \frac{jw}{jw + KA} \tag{3.8}$$

Two aspects are really interesting to observe (see fig.3.13) if A is considered constant:

Error convergence is equal to zero at steady state. Moreover the error is limited to the amplitude fo the reference signal at high frequencies.

Effect of gain K rises the bandwidth virtually to infinite.

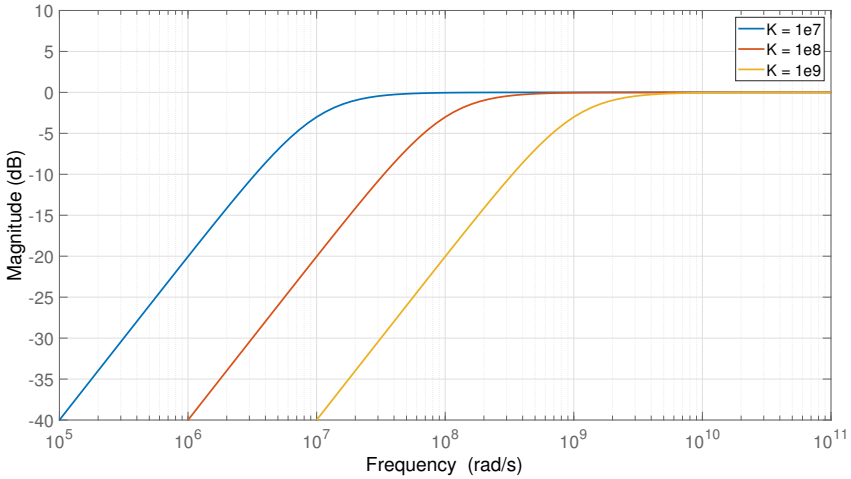

Figure 3.13: Hysteresis compensation. Bode plot of sensitivity function $B(jw)$ with $A = 1$.

Chapter 4

Online Hysteresis identification

This chapter presents an identification algorithm based on the model reported in Chapter2.2. Subsequently, the algorithm is put forward as an adaptive strategy for nonlinear control.

4.1 Recursive algorithm

The identification of the parameters associated with hysteresis behaviour under normal operating conditions represents a significant challenge for model-based control synthesis and tuning approaches. It is noteworthy that only a limited number of recursive methods have been subjected to theoretical analysis and experimental verification for the purpose of online Preisach model identification. This work employs the direct recursive identification method for the Preisach hysteresis model and provides a description of the high efficient-computing discrete-time algorithm for an adaptive hysteresis filter.
It should be recalled that the overall density distribution $\mu_i(\alpha_i, \beta_i)$, for all $i = 1, ..., L$, over the Preisach half-plane determines the shape of input-output hysteresis loops (see fig.2.12) and it is the variable to identified for the given hysteresis system. The discretization process of the Preisach model, as defined by eq.2.9, is applied to the total output. The resulting output of the Preisach hysteresis model is:

$$y(t) = \sum_{P^+} \mu_i(\alpha_i, \beta_i) - \sum_{P^-} \mu_j(\alpha_j, \beta_j) \tag{4.1}$$

The set P^+ is a subset of those hysterons of index i whose instantaneous state is $+1$, while the set P^- is a subset of those hysterons j whose instantaneous state is -1. The direct recursive identification algorithm is

designed to identify the Preisach distribution $\mu(\alpha, \beta)$ based on the estimate $\hat{\mu}(\alpha, \beta)$. The identification algorithm employs the differential output error, defined as $e(k) = y(k) - y(k-1) - \hat{y}(k) + \hat{y}(k-1)$, where $\hat{y}$ represents the output of the adaptive hysteresis filter under identification. The combination of this error with eq.4.1 demonstrates that the differential error is the equivalent mathematical representation of the error in the estimation of the density function $\mu(\alpha, \beta)$:

$$e(k) = \sum_{S^+(k)} (\mu - \hat{\mu}) - \sum_{S^-(k)} (\mu - \hat{\mu}) \tag{4.2}$$

Where we denote those subset of hysterons which switch on, i.e. change their state from -1 to +1 at the time step k by $S^+(k)$ while the subset of hysterons which switch off, i.e. change their state from +1 to -1, is denoted by $S^-(k)$. The direct recursive identification algorithm updates the weight of those hysterons in the switching region $S(k) = S^+(k) \cup S^-(k)$. The update formulation is determined in accordance with the following criteria:

$$\mu_i(k) = \hat{\mu}_i(k-1) + r(k) \tag{4.3}$$

Where $r(k)$ represents the correcting factor, which is described by the following equation:

$$r(k) = \begin{cases} e(k)A(k)^{-1} & \text{if } (\alpha_i, \beta_i) \in S^+(k), \\ -e(k)A(k)^{-1} & \text{if } (\alpha_i, \beta_i) \in S^-(k) \end{cases} \tag{4.4}$$

In this formula, $A(k) = dim(S(k))$ and it represents the number of hysterons within the switching region, which is calculated as the sum of the individual operators $s(k)$ described by the expression:

$$s(k) = 0.5|y(k) - y(k-1)| \tag{4.5}$$

Finally the update law that modifies the hysteron weight is presented.

$$\hat{\mu}_i(k + 0.5) = \hat{\mu}_i(k) + s(k)r(k) \tag{4.6}$$

The block diagram of the adaptive hysteresis filter is presented in Fig.4.1 for the reader's convenience.

Ultimately, it can be demonstrated that the quantity $||\hat{\mu}(k) - \mu||$ is monotonically decreasing for stochastic input processed and almost surely converges to zero exponentially, following the law $Cexp(-\lambda k)$, in the absence of measurement noise. In contrast, in the presence of measurement noise, this quantity converges to a constant residual proportional to the noise power.

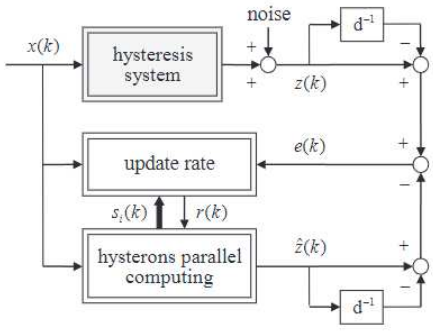

Figure 4.1: Recursive identification algorithm. Blocks diagram (source:[15]).

4.2 Numerical simulations

In this section, a random hysteresis model is constructed for the purpose of analyzing the behaviour and results of the identification process (for the Simulink implementation see AppendixB.1). The algorithm operates at a rate of 2 kHz and reconstructs the hysteresis model using a mesh of 35x35, equivalent to 630 hysterons with a initial uniform density function $\hat{\mu}(k=0) = 1\text{e-}9$. In the initial test, the model is provided with a sinusoidal signal with an amplitude of 5 and a frequency of 1 Hz, with the objective of verifying the identification of the external loop. The results are presented in Fig.4.2.

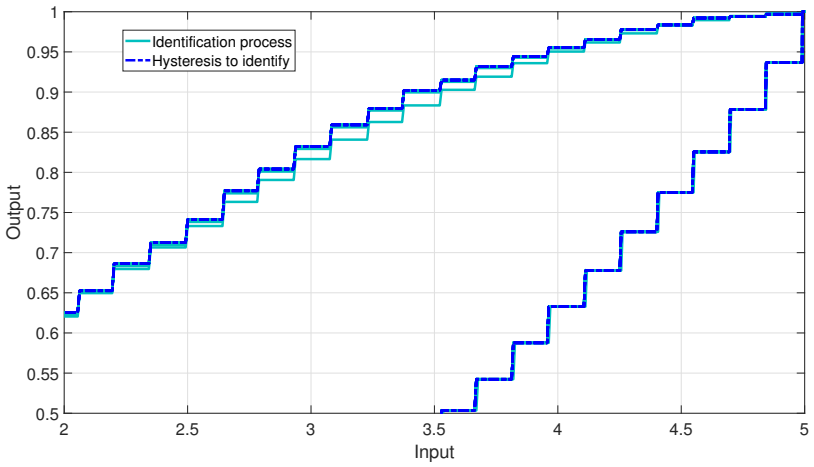

Figure 4.2: Recursive algorithm simulation. This figure illustrates the hysteresis identification process.

A more detailed examination of the identification performance can be conducted by analyzing the time-evolution of the differential error (see fig.4.3).

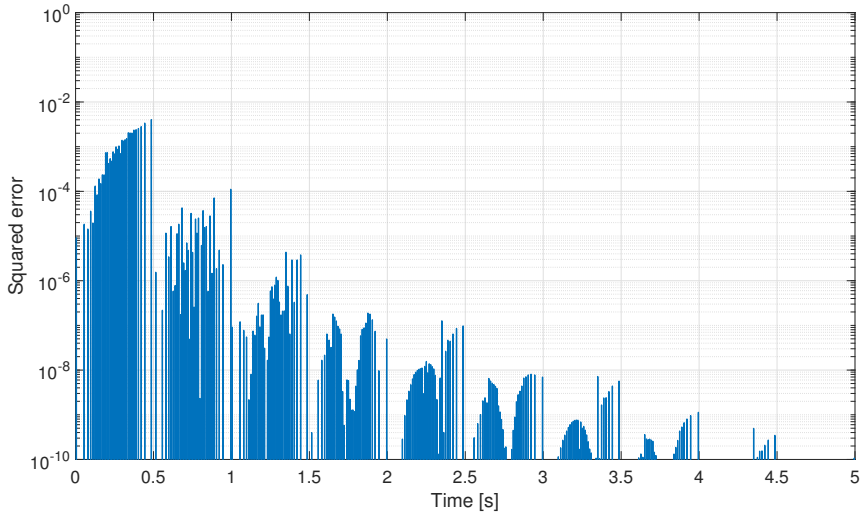

Figure 4.3: Recursive algorithm simulation. Convergence of the error to zero is demonstrated in this picture.

A more detailed examination of the system can be conducted by analyzing the difference in the density function of the two systems at the conclusions of the identification process fig.4.4.

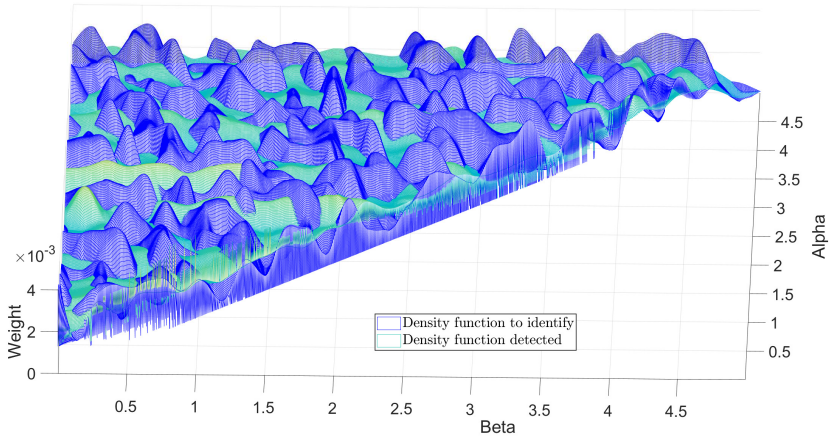

Figure 4.4: Recursive algorithm simulation. The picture illustrates the distinction between two distinct density functions.

In order to obtain a more detailed identification of the hysteresis comprehensive of the internal loop, two additional input signals are employed to test the algorithm. The initial signal is a sine wave exhibiting an increase in amplitude at a frequency of 1 Hz. The subsequent signal is a sinusoidal signal with a non-zero mean, random amplitude, and a frequency of 1 Hz. The temporal evolution of the algorithm and the identified hysteresis are presented in Figure4.5 and Figure.4.6, respectively.

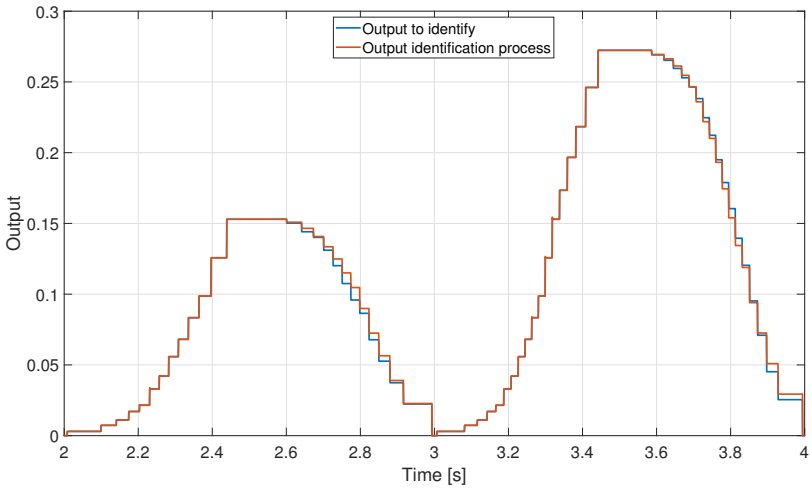

(a) Sinusoidal input with increasing amplitude

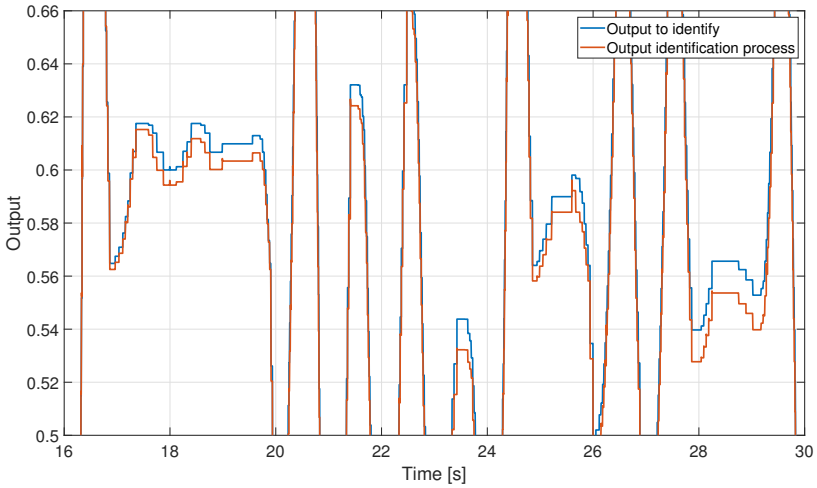

(b) Sinusoidal input with random amplitude

Figure 4.5: Recursive algorithm simulation. Time evolution of the identification process.

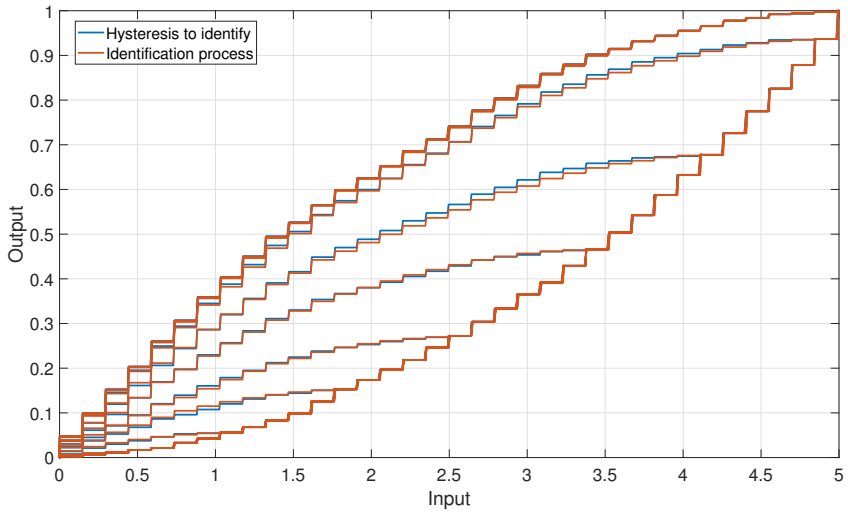

(a) Sinusoidal input with increasing amplitude

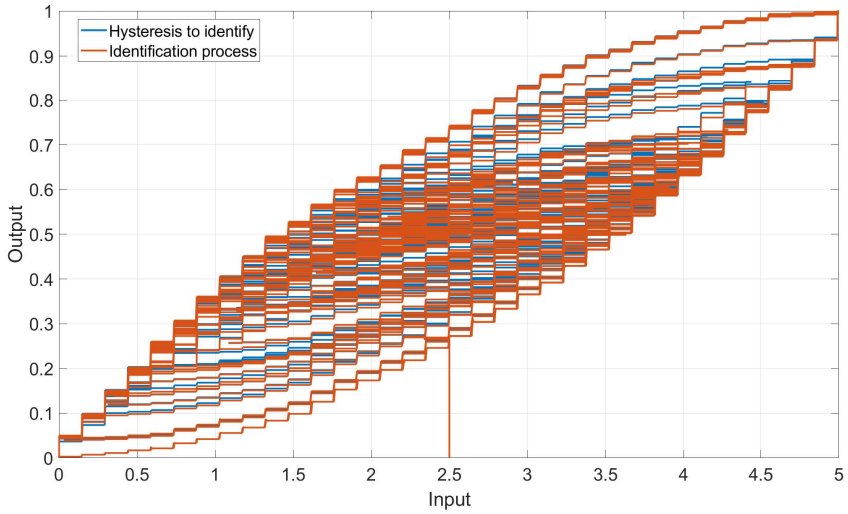

(b) Sinusoidal input with random amplitude

Figure 4.6: Recursive algorithm simulation. Time evolution of the identification process. On the right the vertical line is due to the initial hysteron's weights.

From the figure 4.5 and 4.6, it can be observed that the random input amplitude presents a greater degree of complexity for the algorithmic evaluation. A more accurate comparison can be made by utilizing the differential error as a valuable investigative tool (see fig.4.7).

It is noteworthy that the differential error in Fig.4.7b is unchanging

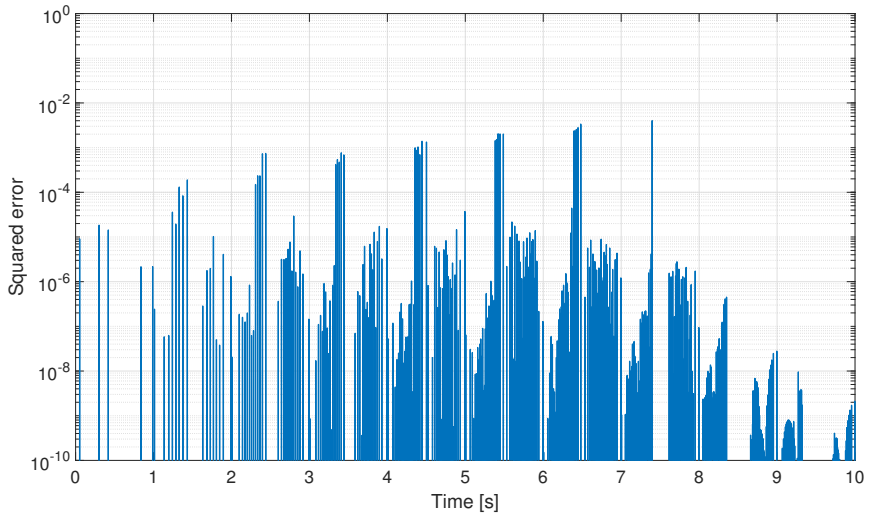

(a) Sinusoidal input with increasing amplitude,

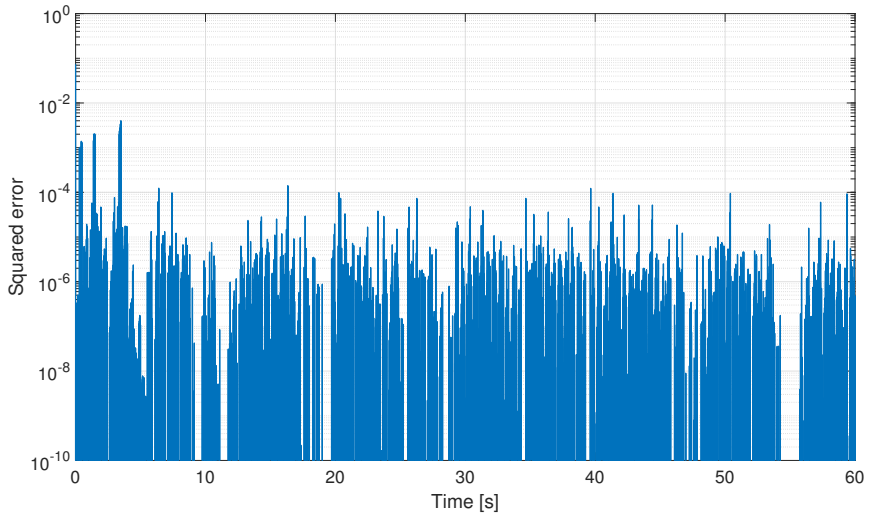

(b) Sinusoidal input with random amplitude,

Figure 4.7: Recursive algorithm simulation. Time evolution of the differential error, that represents a precise accuracy factor of the algorithm.

and attains a steady-state value that is less than that observed in the other case. Furthermore, in Fig.4.7a, a slight increase in the differential error can be observed. This can be attributed to the fact that the algorithm is receiving input values of increasing amplitude for the first time, necessitating a second period for adjustment of the density function within this new region of the Preisach plane. Error values equal to zero have been limited to 1e-10 in order to use this representation.

4.3 Experimental results

To identify the hysteretic behaviour of the MSM element, a triangular input of 0.1 Hz and 5 A amplitude is applied. To better visualize the result (see Fig.4.8), the sensor data is filtered using the same second order low pass filter with a cut-off frequency of 10 Hz as described in eq.3.1.

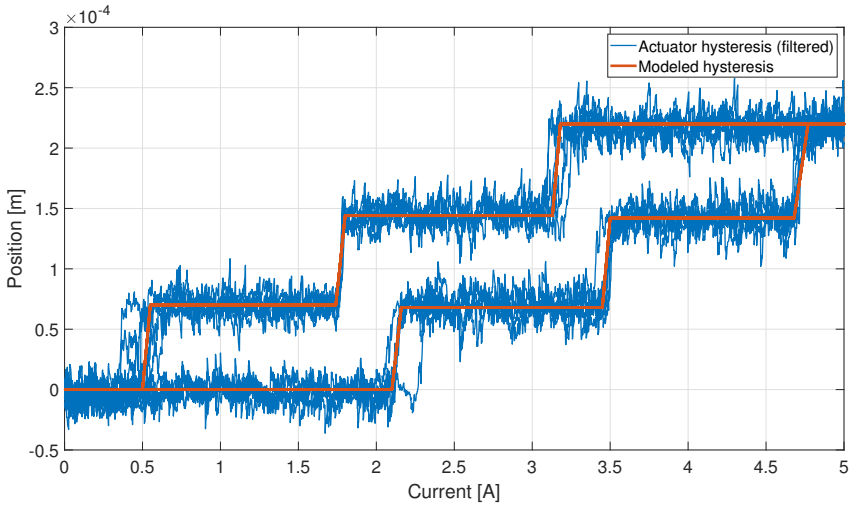

Figure 4.8: Recursive algorithm experiment. Comparison between the hysteresis of the actuator and the modeled hysteresis using the KP model.

This result shows a peculiar hysteresis that can be interpreted as a combination of three different Krasnosel'skii-Pokrovskii (KP) operators. The identification algorithm described in the first section of this chapter is based on Preisach model that described the hysteresis as the superposition of multiple hysterons with same shape but different weights. This representation differs from KP model in which every operator is defined not only by the threshold values (α_i, β_i) and the weight but also from a fourth parameter called slope. This indicates that in order to adequately

describe the hysteresis of the actuator, it is necessary to consider 12 parameters. For this reason this behaviour cannot be identified by the algorithm described in this chapter, whose only degree of freedom is to adjust the density function $\mu(\alpha, \beta)$ on the Preisach plane. This consideration brings to the idea that the easiest way to reproduce this hysteretic response is to use a Matlab script that mimics accurately this behaviour (see AppendixB.2). As example, the identification process is tested on the experimental data signals (Fig.4.9b). The sampling rate is set to 2 kHz and the number of hysterons adapted is L = 630.

As explained before, the shape of the hysteresis of the actuator plays an important role on the identification process. In particular, this characteristic does not allow the algorithm to converge to the exact hysteretic behaviour. It's possible to recognize the shape of the experimental hysteresis but the amplitude of the displacement differs completely. In last analysis, the effect of the filter on the synchronization of the two compared data is presented (see Fig.4.9). It's important to note that the algorithm needs filtered data to identify the hysteresis. This fact suggests that a second filter must be used in the identification branch in order to maintain the synchronization between the signals. This leads to the divergence of the algorithm, which recognizes the shape but cannot identify the correct amplitude of the oscillations.

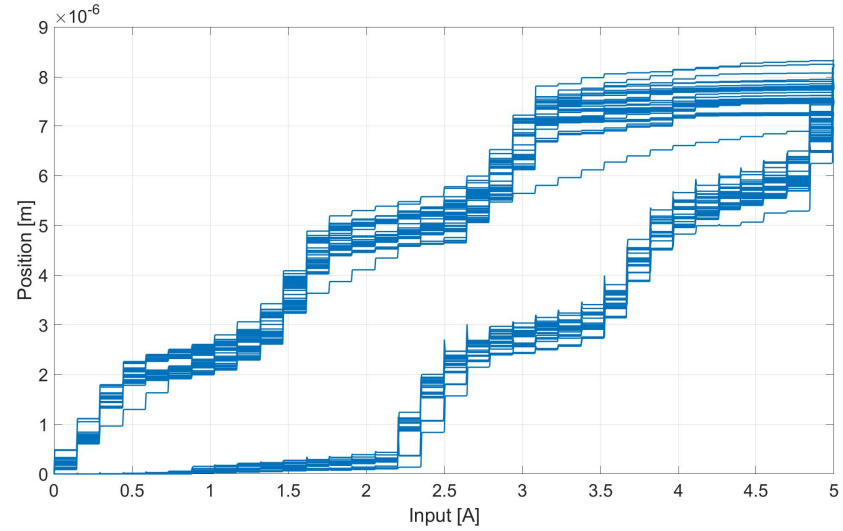

(a) Hysteresis obtained without the filter on the output of the algorithm.

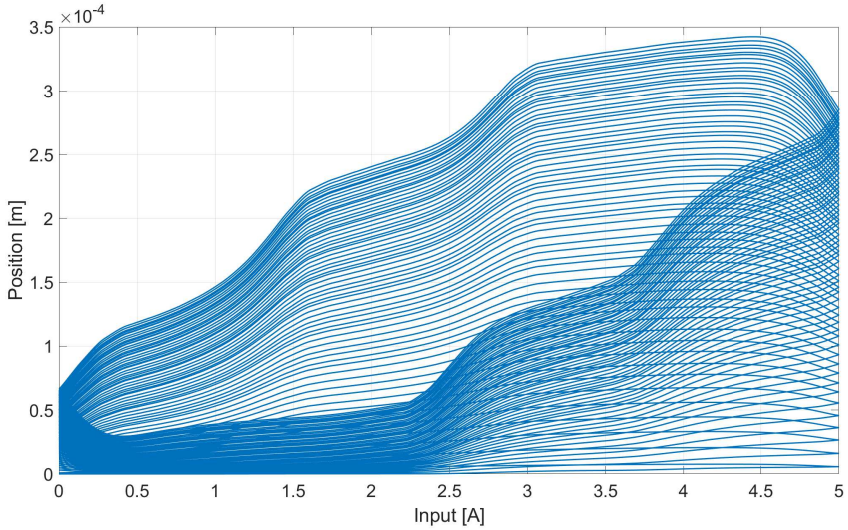

(b) Hysteresis obtained using a filter on the experimental data and another filter on the output of the algorithm.,

Figure 4.9: Recursive algorithm experiment. Effect of the filter on the identification process.

Chapter 5

Control system evaluation

This chapter presents an application of the identification algorithm to propose an adaptive control method that accounts for variations in the hysteresis model over the course of the working period. This approach is purely simulative, and the results and method are presented. Additionally, a fine-tuning of the feedforward compensator is achieved in the simulation environment to obtain optimal control results using a combination of feedforward and feedback. Finally, the experimental results are reported.

5.1 Adaptive control simulation (smooth hysteresis)

The objective of this section is to present an adaptive strategy for the nonlinear control of hysteretic actuators. This approach is fundamental for all applications where time and operational conditions have a significant impact on actuator behaviour. As outlined in Chapter3.3, the feedforward mechanism requires an accurate model of the hysteresis to compensate it. For this reason, the recursive algorithm presented in Chapter4 is introduced herewith. The combination of these two methods promises to avoid waste in terms of time and energy on the identification of the hysteresis model, thereby obtaining a more reliable control system. This process can be fully automated and integrated to obtain an online correction on the control system (for the Simulink scheme go to AppendixB.3). In consideration of the identification issues presented in Chapter4.3, a simulated hysteresis is considered (see Fig.5.1).

The simulation is conducted with 630 hysterons at a sampling rate of 2 kHz and can be divided into two phases. The initial phase comprises the identification process, which utilizes a random input signal and has

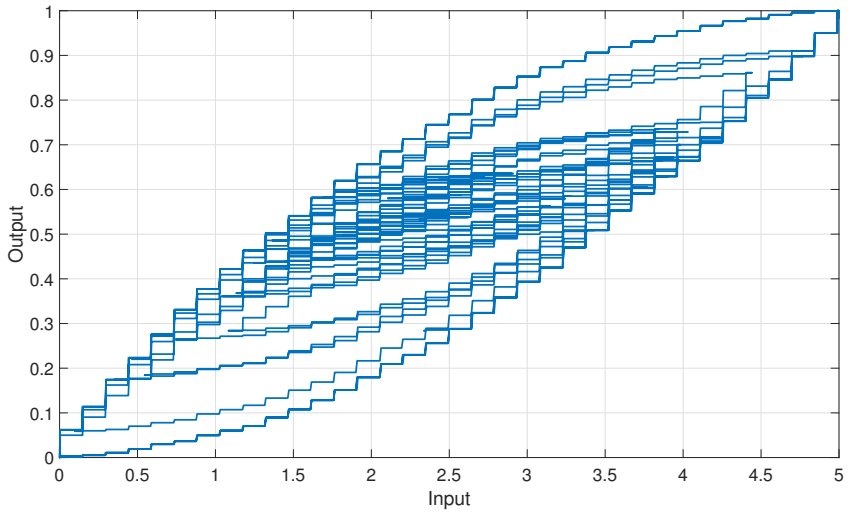

Figure 5.1: Adaptive control. Hysteresis model to control.

a duration of 30 seconds (see Fig.5.2). The second phase comprises the control process, which employs a feedforward with an integral gain K. The results are reported in Fig.5.3.

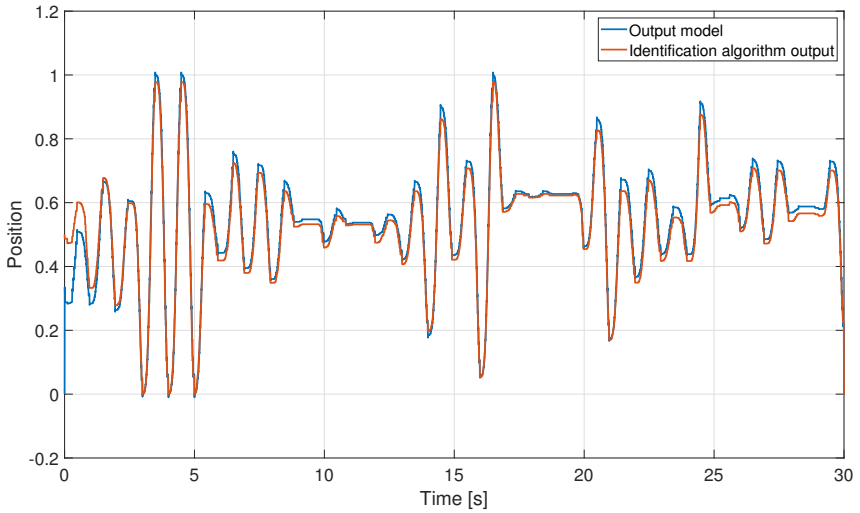

Figure 5.2: Adaptive control. Identification process.

The mean square error (MSE) represents an effective index for benchmarking the performance of the system. The value is calculated within the time range [46-48] seconds and is compared with a series of different

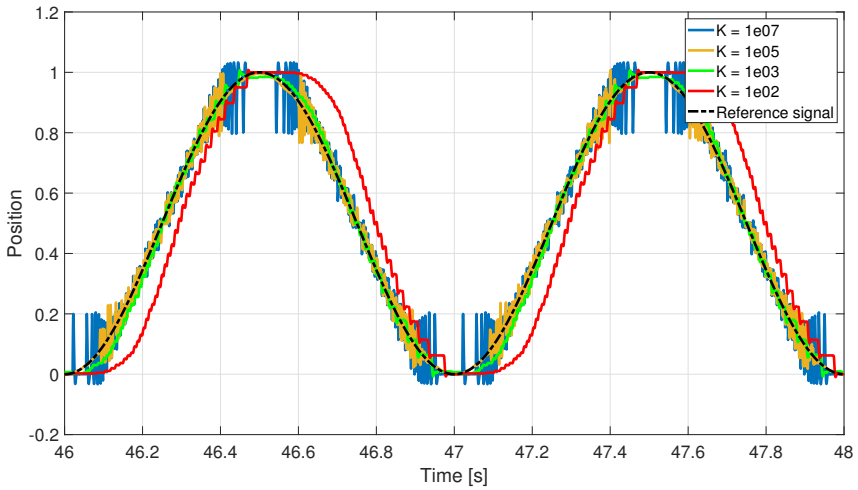

Figure 5.3: Adaptive control. Effect of the integral gain in the hysteresis compensation block.

values of gain K (see Tab.5.1).

Feedforward integral gain	Mean Square Error $[mm^2]$
K = 1e02	0.0153
K = 1e03	4.9756e-04
K = 1e04	0.0020
K = 1e05	6.9490e-04
K = 1e07	0.0021

Table 5.1: Adaptive control. Mean Square Error of the adaptive simulation comparing the different gain K.

Table5.1 clearly indicates that the optimal choice for the integral gain is 1e03. This result is consistent with the findings in Fig.5.3, which demonstrate that a high value of K has a positive impact on not only the hysteresis compensation but also on reducing the lag between the reference signal and the obtained output. Conversely, this degree of accuracy gives rise to oscillatory behaviour. The optimal compromise between accuracy and oscillations is achieved with K = 1e03, where the oscillations are almost absent and the output lag is negligible. At the end, the combined effect of feedforward and feedback loop is illustrated in Fig.5.4.

From Fig.5.4 is clear that the PI regulator has a negative effect on

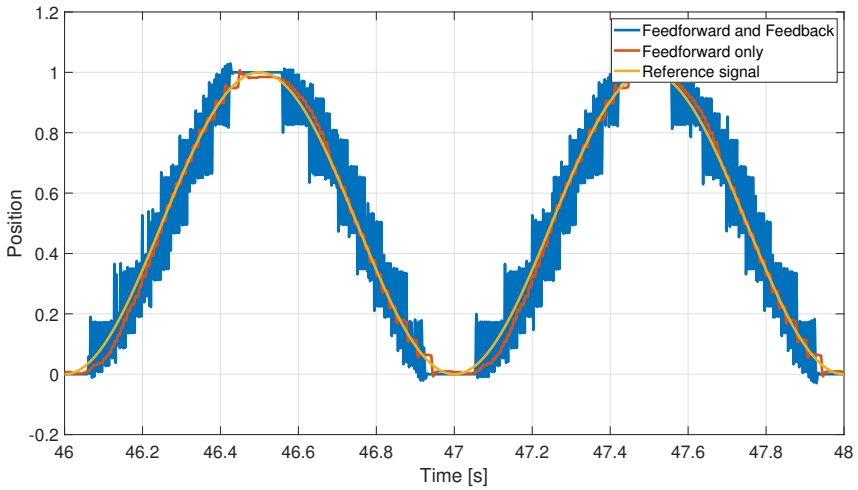

Figure 5.4: Adaptive control. Effect of the feedback loop on the adaptive system with K = 1e03.

the control loop. It's important to remark that this result is completely explainable in the simulation environment but for practical applications a feedback loop is always adopted in order to correct any error in the identification process.

5.2 Control system tuning (non-smooth hysteresis)

As evidenced in the preceding section, once the PI regulator has been designed, the integral gain of the hysteresis compensator represents the final parameter to be tuned. The goal of this section is to utilize the simulation tool in order to minimize the control error quantity. The simulation runs at 2 kHz and in the feedforward block, the Matlab script that was previously discussed, is employed. The actuator behaviour is simulated by connecting in series the hysteresis script and the normalized version of transfer function $G(s)$, in order to simulate the oscillatory behaviour on the real system (see AppendixC.1). The first attempt of tuning is achieved comparing the open-loop performances with different gains K, the results are reported in Fig.5.5.

In Fig.5.5 it is possible to observe that the optimal result is achieved with a gain K = 3e06. A higher gain K = 1e07 results in a very oscillating response of the system while a lower one, K = 1e06, cannot compensate

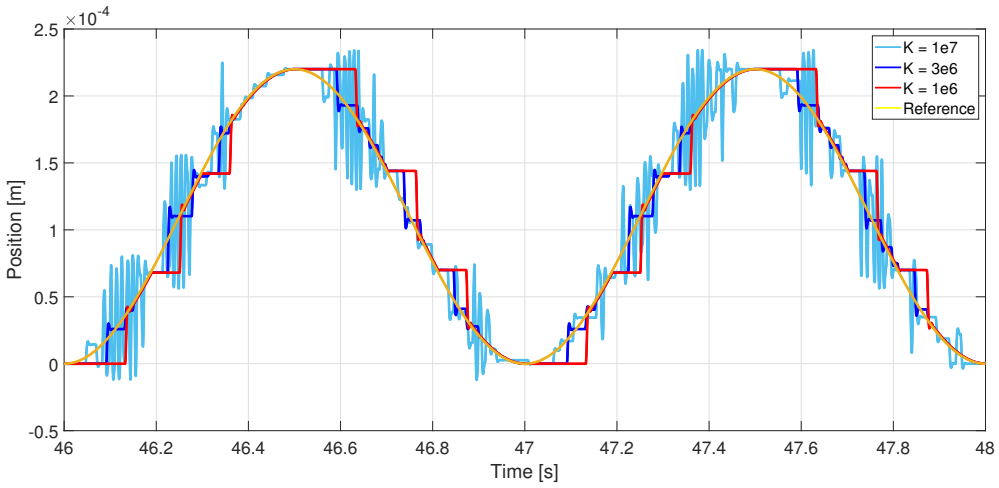

Figure 5.5: Tuning. Effect of the gain K in the feedforward-based control system.

properly the steps of the hysteresis behaviour. The combination of feedback and feedforward is now analyzed using the results reported in Fig.5.6.

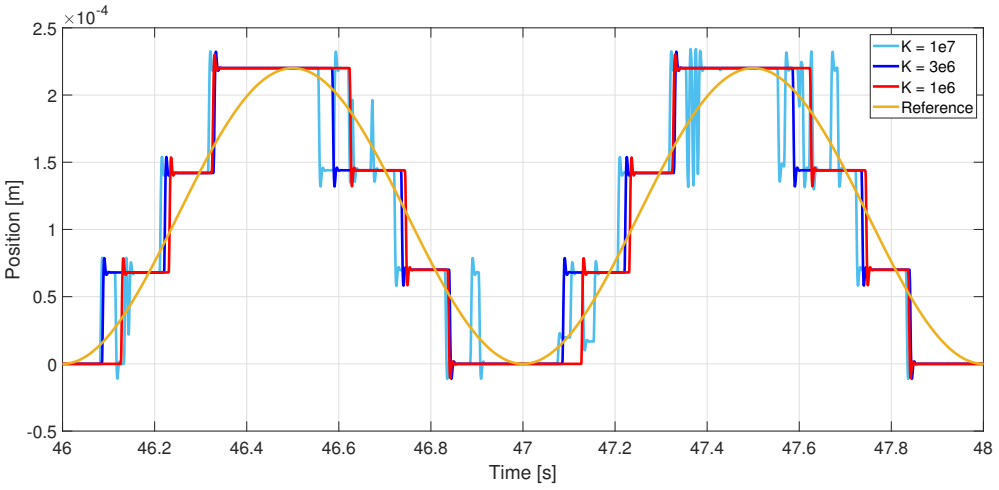

Figure 5.6: Tuning. Effect of the gain K on the combination of feedback and feedforward.

In Fig.5.6 it's possible to notice that the combination between PI regulator and hysteresis compensator results damaging for the system. To compare these solutions the MSE of every different experiments are re-

ported in Tab5.2.

Feedforward integral gain	Mean Square Error $[mm^2]$
K = 1e06	9.33e-07
K = 3e06	1.23e-06
K = 1e07	1.58e-06

Table 5.2: Tuning. Mean Square Error of the simulation with both feedback and feedforward in the period [46-48] seconds.

As evidenced by the MSE data, the optimal configuration is attained with K = 1e06. The influence of the integral gain K can be elucidated by a more pronounced contribution of the hysteresis compensator, which operates independently of the PI regulator. This leads to a command input that induces oscillatory behaviour in the output position between the various levels of the hysteresis.

5.3 Simulated control results

This section presents more detailed results concerning different configurations of the control system model. Given the superior response achieved through the combination of feedback and feedforward control, the integral gain K = 1e06 is employed. The validation references are sinusoidal waves (Fig.5.7), a slope (Fig.5.8), and two steps (Fig.5.9).

The results in Fig.5.7 are better described using the MSE quantity reported in Tab.5.3.

Control system Technique	Reference signal [mm]	Mean Square Error $[mm^2]$
Feedback	0.22	5.6301e-10
Feedforward	0.22	2.3564e-10
Feedback + Feedforward	0.22	4.6565e-10
Feedback	0.1	5.3810e-10
Feedforward	0.1	1.0567e-10
Feedback + Feedforward	0.1	8.5738e-10

Table 5.3: Control system simulation. Mean Square Error with sinusoidal input into the period [46-48] seconds.

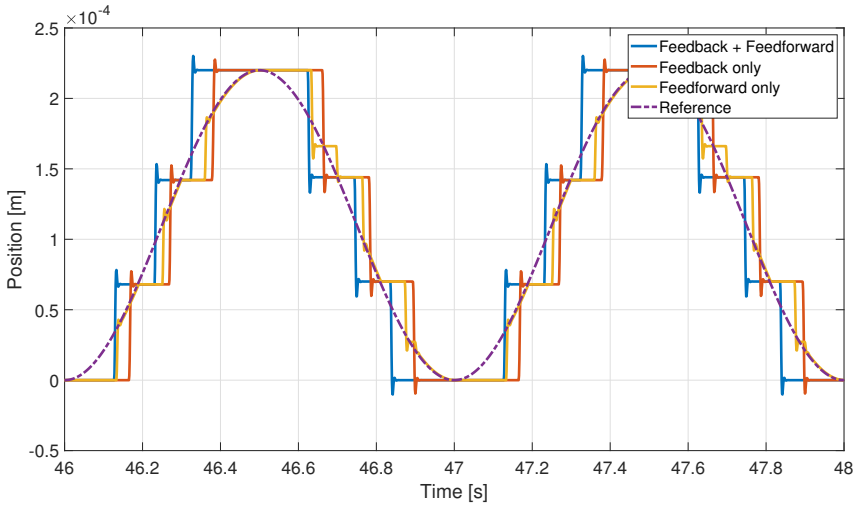

(a) Sinusoidal reference signal with amplitude 0.22 mm.

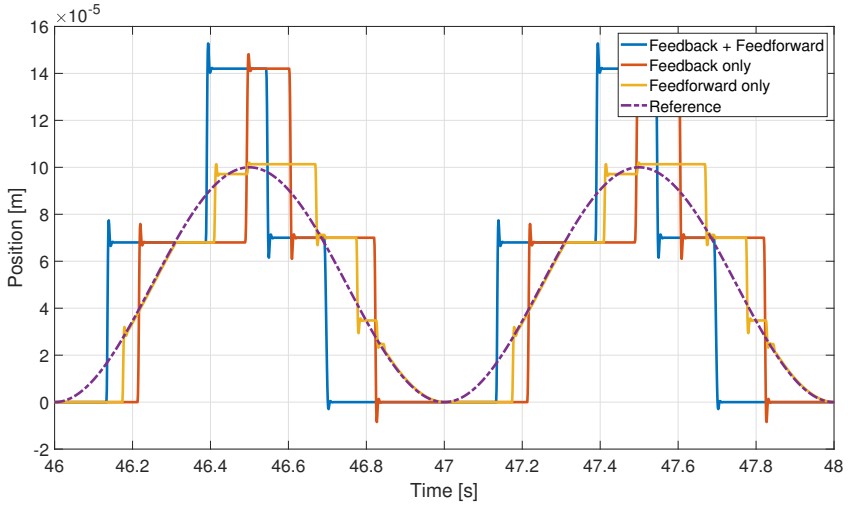

(b) Sinusoidal reference signal with amplitude 0.1 mm.

Figure 5.7: Control system simulation. Sinusoidal reference signals.

From Tab.5.3 it can be observed that, in all of the tested conditions, the system that is regulated using the feedforward method exhibited the best performance. On the other hand, the combined effect of feedforward and feedback is deleterious to the system when the reference amplitude is at its lowest level.

In Fig.5.8 it's possible to observe that the only action of the feedforward is enough to follow almost perfectly the trajectory of the reference signal. Moreover, also in this case, the effect of feedback with feedforward is worse

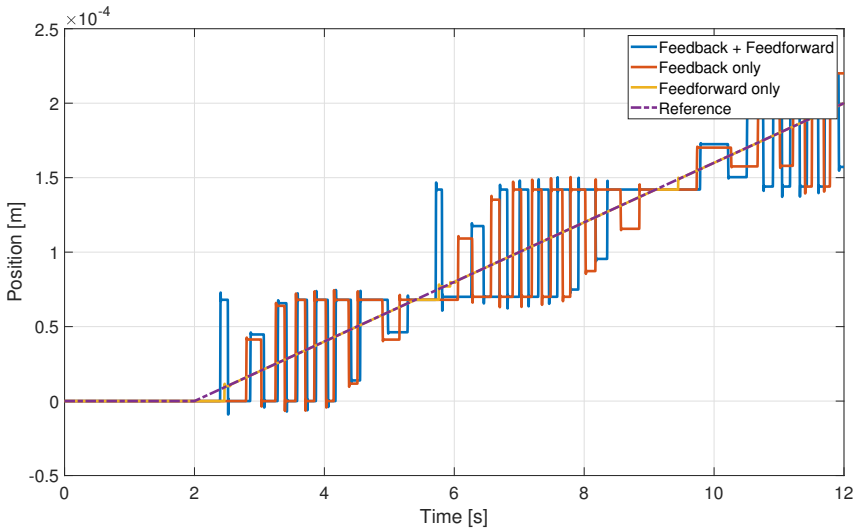

Figure 5.8: Control system simulation. Slope reference signal.

than the case with only feedback.

Additionally, Fig.5.9 illustrates that the feedforward approach achieves optimal results due to the precise modelling of hysteresis. Furthermore, the figure demonstrates that a limit cycle is generated by the PI regulator contribution.

5.4 Experimental results

In this concluding section, the control theory that has been previously studied and applied in the simulations is subjected to practical tests. The PI regulator transfer function is the same described in eq.3.3 and the KP model represented in Fig.4.8 is used for the hysteresis compensation. In the initial experimental phase a final test is conducted to determine the optimal value of K (Fig.5.10), a comparison is made between all possible combinations of the three different techniques of control (feedforward, feedback and the combination of both), and all of this is done using the different reference signals with varying amplitude (for the implementation using Simulink go to AppendixC.2). Furthermore, a comparison of the three control method energetic consumption is provided.

Fig.5.10 illustrates the utilization of a feedback and feedforward combination to tune the integral gain K. This approach is necessitated by the need to optimize the integration of the feedforward with the fundamental feedback loop control. The results demonstrate that, in instances where

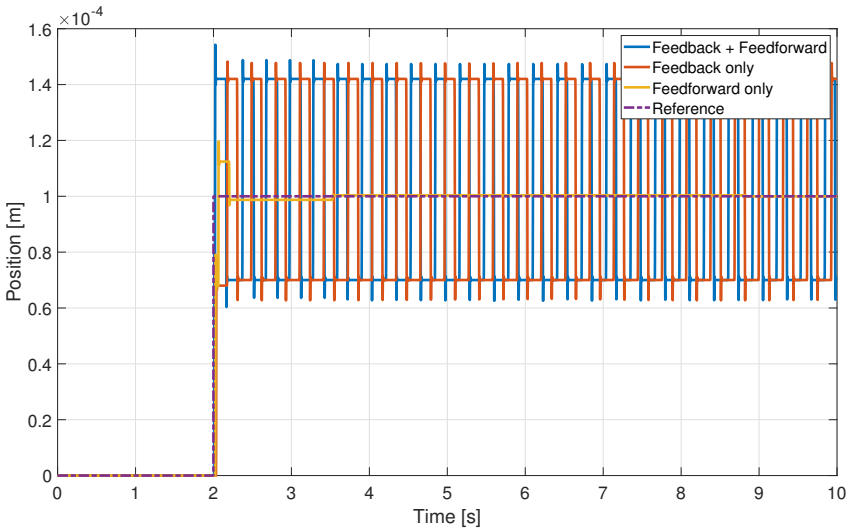

(a) Step reference signal with amplitude 0.2 mm.

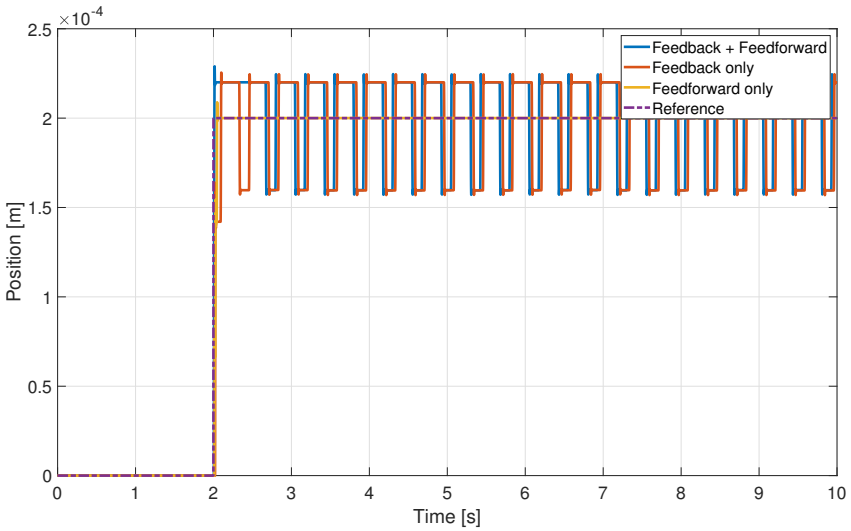

(b) Step reference signal with amplitude 0.1 mm.

Figure 5.9: Control system simulation. Step reference signals.

the amplitude of the reference signal is high, the variation in K is relatively minimal. Conversely, in scenarios where the requested displacement is smaller, a higher gain of K = 1e07 is more suited to better align with the reference. Accordingly, this value will be incorporated into future experiments.

As illustrated in Fig.5.11, the combination of feedforward and feedback

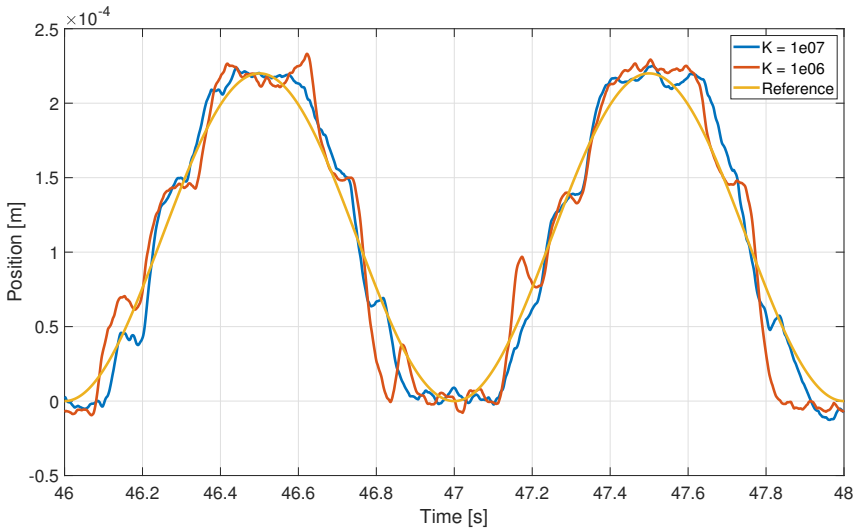

(a) Sinusoidal reference signal with amplitude 0.22 mm.

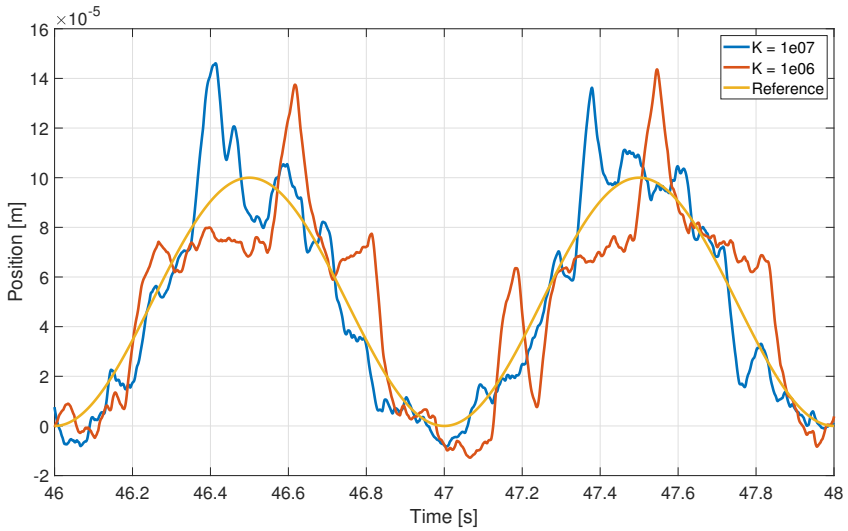

(b) Sinusoidal reference signal with amplitude 0.1 mm.

Figure 5.10: Control system experiment. Tuning of the integral gain K (filtered data).

mechanisms yields the most optimal outcome. In particular, the feedback mechanism plays a significant role in correcting the inaccuracies inherent to the model and compensating for the impact of external factors. In light of the preceding considerations, the case of pure feedforward will no longer be presented.

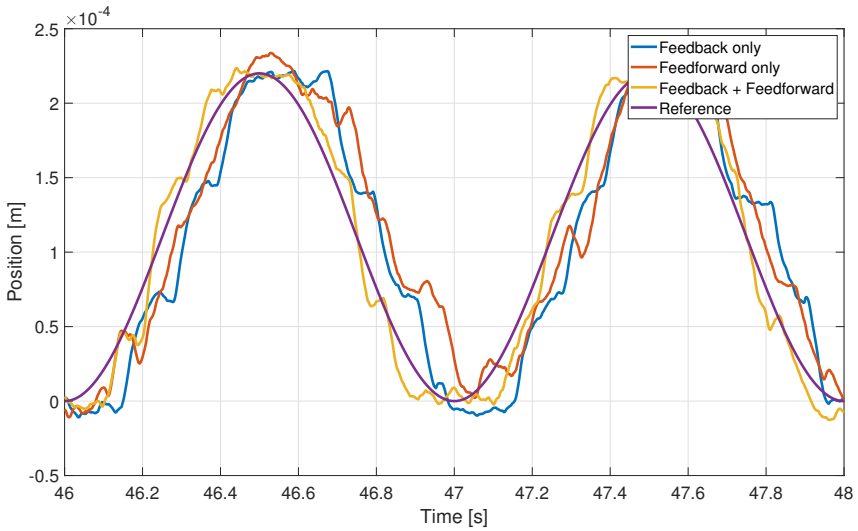

(a) Sinusoidal reference signal with amplitude 0.22 mm.

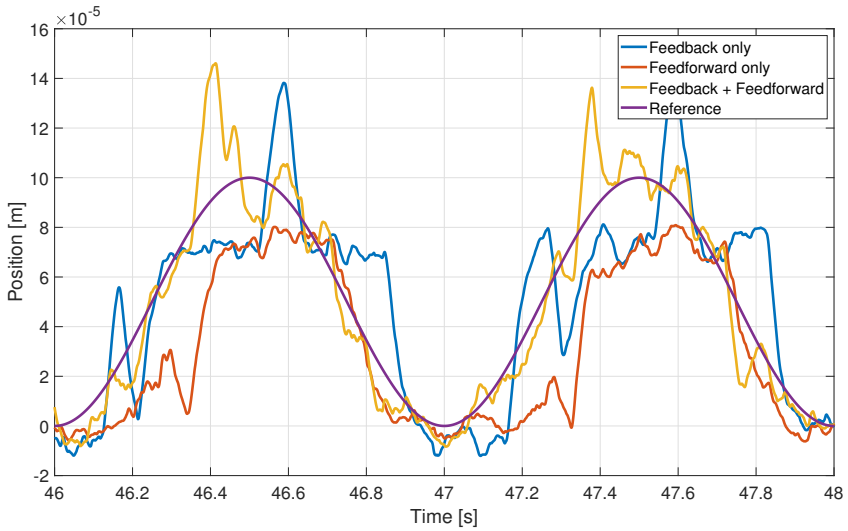

(b) Sinusoidal reference signal with amplitude 0.1 mm.

Figure 5.11: Control system experiment. Sinusoidal reference input (filtered data).

As in the preceding test, Fig.5.12 demonstrates that the effect of the feedback contributes to an improvement in performance. The last example of reference signal is the step, in particular two different steps are provided in order to better analyze the behaviour of the system (see Fig.5.13).

Ultimately, the Tab5.4 was employed to examine the energy consump-

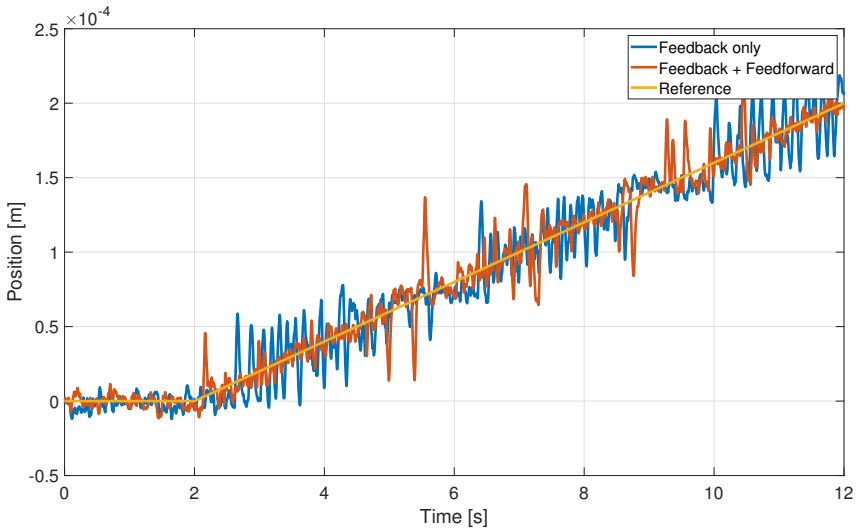

Figure 5.12: Control system experiment. Slope reference signal.

tion between the PI-only regulation and the combination of the two methods. The expression used to calculate this index is:

$$E(T) = \sum_{t=0}^{T} i_{tot}^2(t)\Delta t \tag{5.1}$$

Where T is the operation time and i_{tot} is the control signal.

Control system Technique	Reference signal	Control cost $[A^2s]$
Feedback	Sinusoidal 0.22 mm	567.80
Feedback + Feedforward	Sinusoidal 0.22 mm	615.29
Feedback	Sinusoidal 0.1 mm	229.49
Feedback + Feedforward	Sinusoidal 0.1 mm	305.26
Feedback	Slope 0.2 mm	80.50
Feedback + Feedforward	Slope 0.2 mm	81.63
Feedback	Step 0.2 mm	151.32
Feedback + Feedforward	Step 0.2 mm	124.62
Feedback	Step 0.1 mm	91.57
Feedback + Feedforward	Step 0.1 mm	57.91

Table 5.4: Control system experiment. Index of the energy consumption during the entire test.

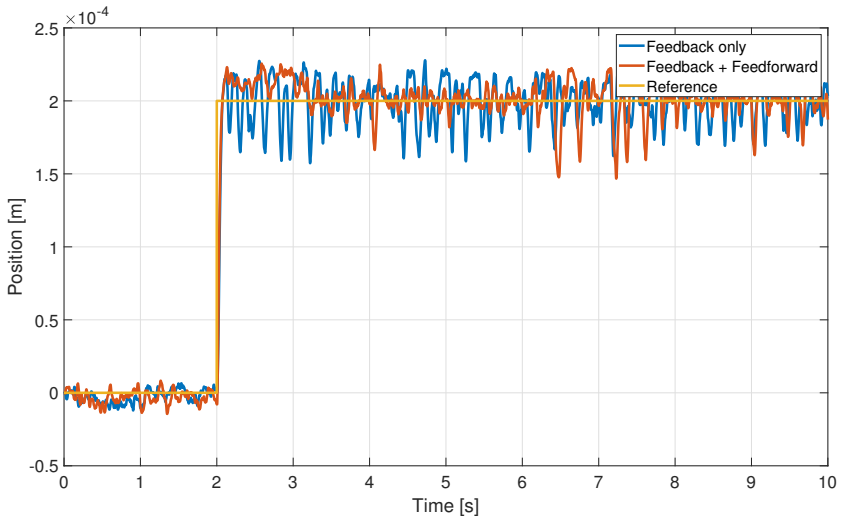

(a) Step reference signal with amplitude 0.2 mm.

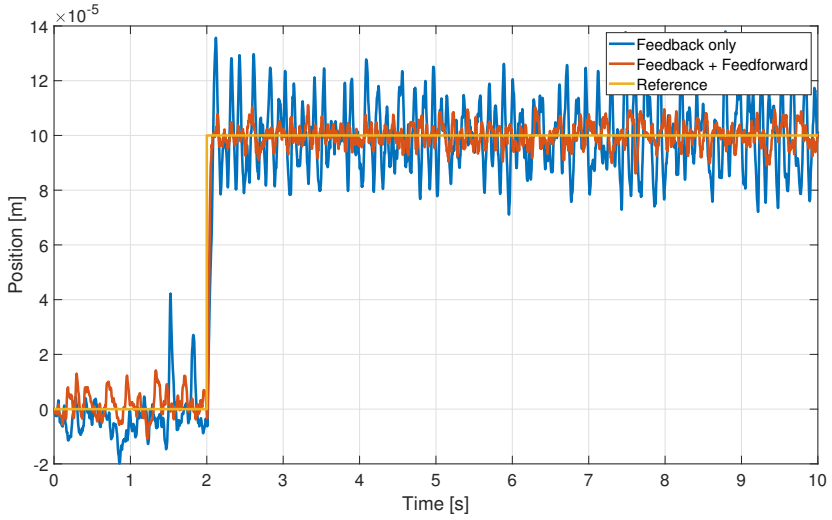

(b) Step reference signal with amplitude 0.1 mm.

Figure 5.13: Control system experiment. Step reference input (filtered data).

In conclusion, an analysis of the results presented in Tab5.4 is reported. Firstly, high dynamics result in a greater energy consumption by the hysteresis compensator. This effect is less pronounced in the slope case, where the energy consumption is nearly identical. Secondly, a steady-state, represented by the step response, leads to a greater energy consumption by the PI regulator due to the limit cycle.

Conclusions and discussion

This thesis examined the potential of adaptive strategies for the linear and nonlinear control of actuators based on MSM materials. MSMs represent a promising technology for position control; however, their strong nonlinearity, particularly the hysteretic behaviour, presents significant challenges for practical applications.

Hysteresis Modeling

The adoption of the Preisach model provided a robust representation of the hysteretic behaviour of MSM actuators, demonstrating an efficacy in describing complex hysteresis cycles, including the wiping-out property. The model is particularly well-suited for the description of rate-independent phenomena, offering computational efficiency in real-time applications.

Identification algorithm

Simulation results

The developed recursive algorithm proved highly effective in simulation. Under ideal conditions, without added noise, the algorithm showed excellent adaptability to the Preisach model, with the differential error converging quickly to negligible values.

Experimental limitations

During the experimental phase of the study, the algorithm was unable to accurately identify the true behaviour of the actuator. Despite the compensation for the delay introduced by data filtering, the discrepancy between the identified model and the measured behaviour remained. This

discrepancy was attributed to the greater complexity of the experimental hysteretic behaviour, which includes phenomena not captured by the adopted model.

Experimental validation

System analysis

The results of the experimental tests confirmed that the theoretical model of the actuator is an accurate representation of the observed behaviour. The observed responses were found to be in accordance with the model's predictions, exhibiting no notable discrepancies.

Effect of Feedback and Feedforward

The combination of feedforward and feedback control was found to be an effective method for improving overall performance. The feedforward compensator facilitated a reduction in tracking error, while the feedback mechanism ensured robustness and compensated for uncertainties. The results of the energetic analysis demonstrated that during the steady-state, the feedforward compensator serves to reduce the necessity for corrections by the PI controller, thereby limiting the occurrence of current peaks and overall consumption. However, under specific operating conditions, the extensive utilization of feedforward may result in an increased level of energetic consumption.

Implications and Future Developments

This work demonstrates the potential of MSM actuators but also identifies the challenges associated with their practical implementation, particularly in the context of complex hysteresis. To address the current limitations, the following research directions are proposed:

Advanced Modeling: The adoption of alternative or complementary approaches to the Preisach model, such as hybrid models or machine learning techniques, may facilitate a more accurate representation of the hysteretic characteristics observed experimentally.

Control Optimization: The integration of advanced control techniques is employed to enhance the synergy between feedforward and feedback, thereby preventing the occurrence of unwanted oscillations.

Further research could investigate the potential of adaptive compensators to adaptively adjust to variations in system behaviour.

Extension of experiments: Expanding experimental conditions, such as including temperature and frequency variations, to assess the robustness of the control and the model in more realistic scenarios.

This work represents a significant advancement in our comprehension of and capacity to regulate MSM actuators. Despite its limitations, the study demonstrated the possibility of implementing adaptive control strategies and contributed to the foundation for future developments, which could facilitate the practical application of this technology in industrial and technological contexts.

Bibliography

[1] J.-H. Lin and M.-H. Chiang, "Tracking control of a magnetic shape memory actuator using an inverse preisach model with modified fuzzy sliding mode control," *Sensors*, vol. 16, no. 9, p. 1368, 2016.

[2] J. Tellinen, I. Suorsa, A. Jääskeläinen, I. Aaltio, and K. Ullakko, "Basic properties of magnetic shape memory actuators," in *8th international conference ACTUATOR*, vol. 2002, pp. 10–12, 2002.

[3] K. Ullakko, "Magnetically controlled shape memory alloys: A new class of actuator materials," *Journal of materials Engineering and Performance*, vol. 5, pp. 405–409, 1996.

[4] K. Ullakko, J. Huang, C. Kantner, R. Oâhandley, and V. Kokorin, "Large magnetic-field-induced strains in ni2mnga single crystals," *Applied Physics Letters*, vol. 69, no. 13, pp. 1966–1968, 1996.

[5] H. T. Banks and A. Kurdila, "Hysteretic control influence operators representing smart material actuators: identification and approximation," in *Proceedings of 35th IEEE Conference on Decision and Control*, vol. 4, pp. 3711–3716, IEEE, 1996.

[6] N. Sarawate and M. Dapino, "Frequency dependent strain-field hysteresis model for ferromagnetic shape memory ni–mn–ga," *IEEE transactions on magnetics*, vol. 44, no. 5, pp. 566–575, 2008.

[7] F. Ehle, S. Stark, P. Neumeister, and H. Neubert, "A thermodynamically consistent lumped-element model for magnetic shape memory components," *Journal of Intelligent Material Systems and Structures*, vol. 34, no. 12, pp. 1389–1405, 2023.

[8] M. Ruderman and T. Bertram, "Discrete dynamic preisach model for robust inverse control of hysteresis systems," in *49th IEEE Conference on Decision and Control (CDC)*, pp. 3463–3468, IEEE, 2010.

[9] R. V. Iyer and X. Tan, "Control of hysteretic systems through inverse compensation," *IEEE Control Systems Magazine*, vol. 29, no. 1, pp. 83–99, 2009.

[10] M. Ruderman and T. Bertram, "Control of magnetic shape memory actuators using observer-based inverse hysteresis approach," *IEEE Transactions on Control Systems Technology*, vol. 22, no. 3, pp. 1181–1189, 2013.

[11] M. Ruderman and T. Bertram, "On system-oriented modeling and identification of magnetic shape memory (msm) actuators," in *2011 19th Mediterranean Conference on Control & Automation (MED)*, pp. 1134–1139, IEEE, 2011.

[12] I. Mayergoyz, "Mathematical models of hysteresis," *IEEE Transactions on Magnetics*, vol. 22, no. 5, pp. 603–608, 1986.

[13] M. Ruderman, "Computationally efficient formulation of relay operator for preisach hysteresis modeling," *IEEE Transactions on Magnetics*, vol. 51, no. 12, pp. 1–4, 2015.

[14] M. Ruderman, "Inversion-free feedforward hysteresis control using preisach model," in *2023 European Control Conference (ECC)*, pp. 1–6, IEEE, 2023.

[15] M. Ruderman and D. Rachinskii, "Discrete-time adaptive hysteresis filter for parallel computing and recursive identification of preisach model," in *2018 IEEE Conference on Control Technology and Applications (CCTA)*, pp. 1096–1101, IEEE, 2018.

List of Tables

List of Figures

Appendix A

Hysteresis modeling

A.1 Matlab Code for the initialization of the Preisach plane

```
1
2       %% Definition of hysterons' parameters
3       N = 35;
4
5       hysteron.alfa = (linspace(4.99, 0.001, N))';
6       hysteron.beta = (linspace(0.001, 4.99, N))';
7
8       hysteron.initial_value = -1;
9       hysteron.initial_weight = 1e-9;
10
11      d = ((N*N)+N)/2;
12      hysteron.real_weights = (1-(hysteron.
           initial_weight)).*rand(d,1) + hysteron.
           initial_weight;
13      s = sum(hysteron.real_weights, "all");
14      hysteron.real_weights = hysteron.real_weights/s
           ;
15      s_new = sum(hysteron.real_weights, "all");
16
17      %% Preisach plane
18      d = 0;
19      for i = 1:N
20      for j = 1:N-i+1
21      d = d+1;
22      hysteron.bound(d,1) = hysteron.alfa(i,1);
```

```
23          hysteron.bound(d,2) = hysteron.beta(j,1);
24          end
25          end
26
27          hysteron.alfa = hysteron.bound(:,1);
28          hysteron.beta = hysteron.bound(:,2);
```

A.2 Simulink scheme of the hysteresis modeling

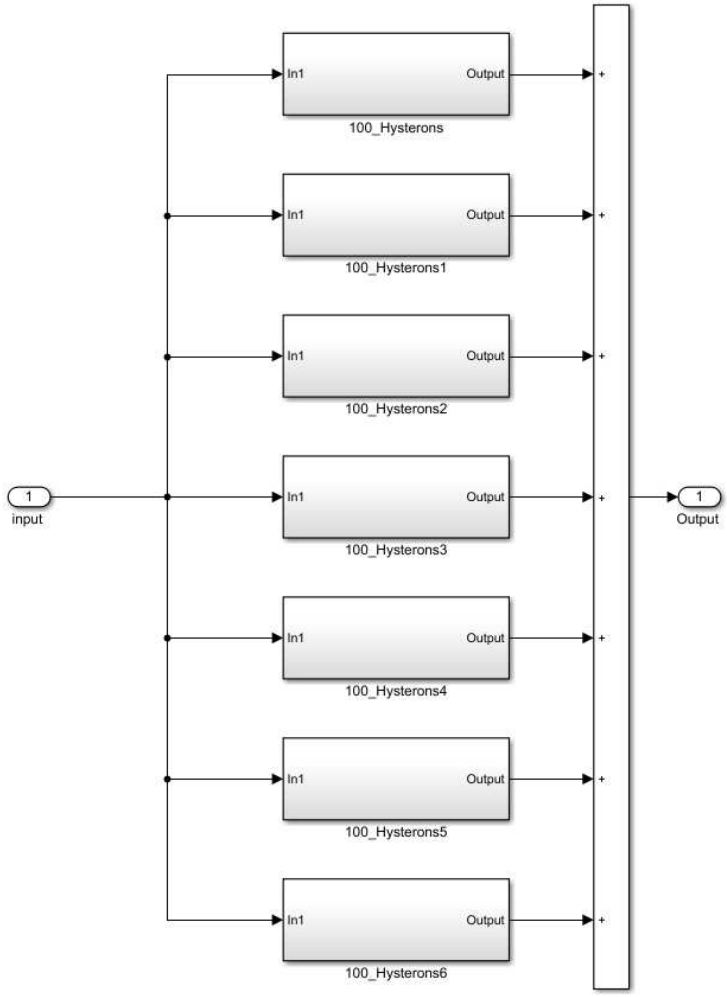

Figure A.1: Most external part of the model. L = 630 hysterons.

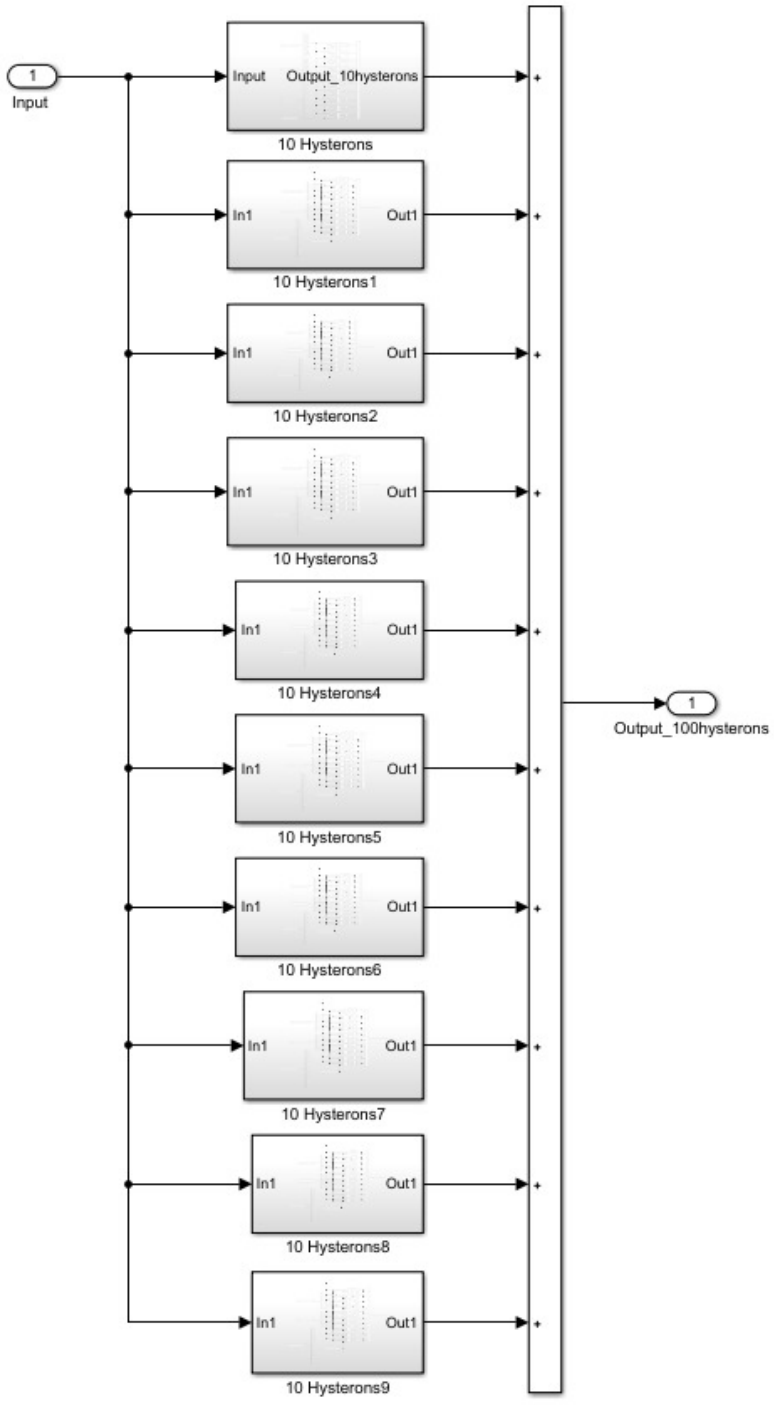

Figure A.2: Second layer of the model. Aggregate of 100 hysterons.

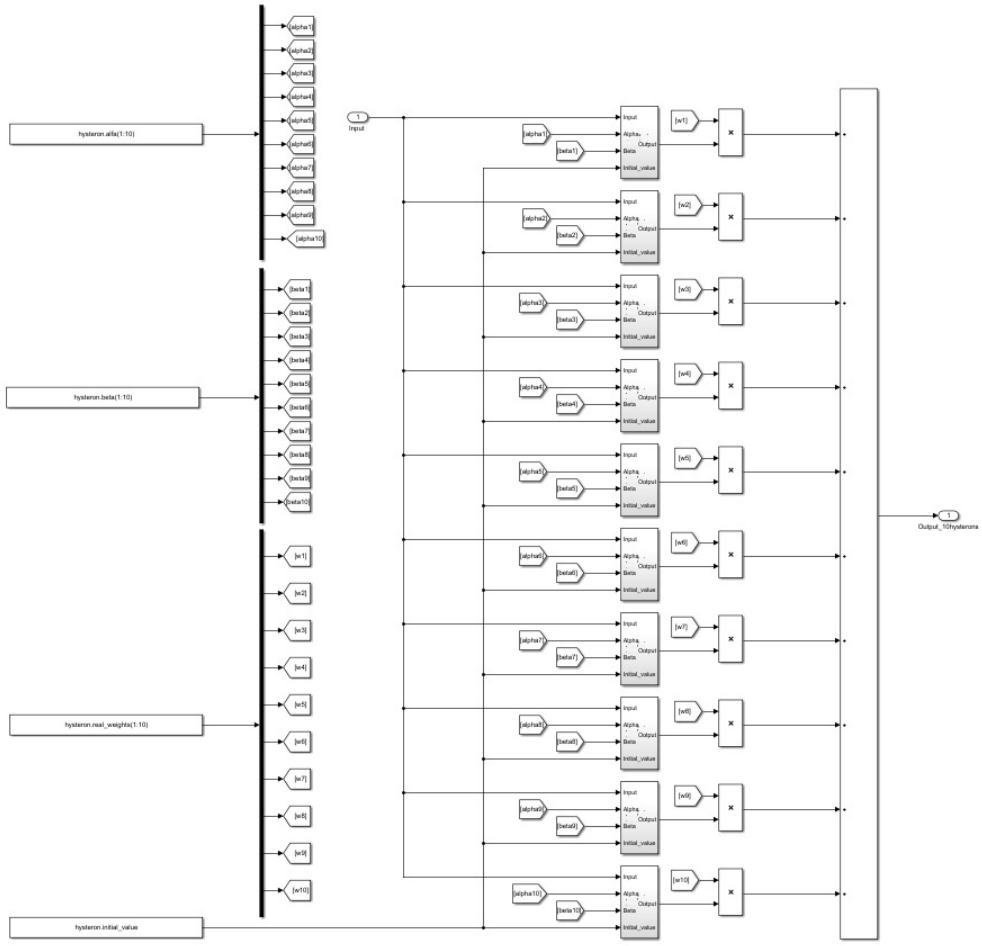

Figure A.3: Third layer of the model. Composition of 10 hysterons. Here the threshold value alpha, beta and the weight to every hysteron are provided.

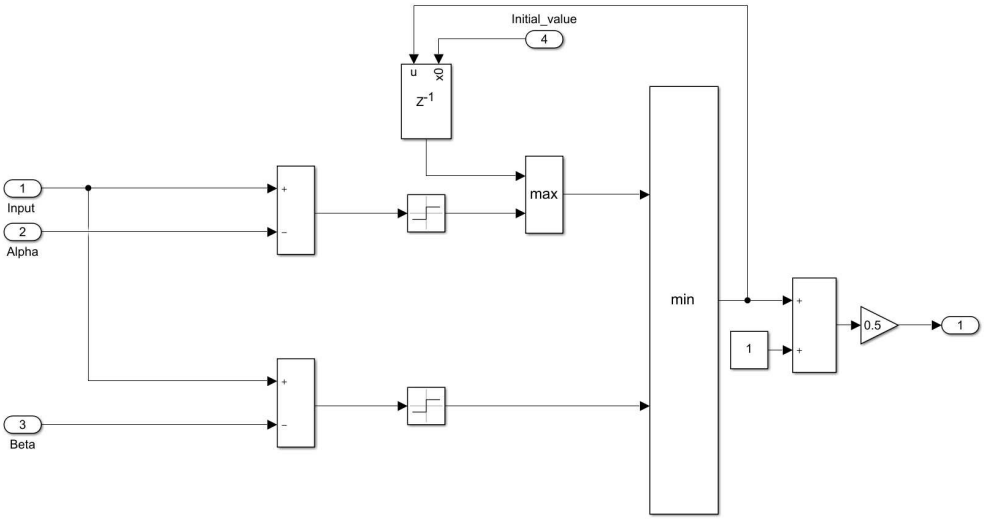

Figure A.4: Simulink scheme of a single hysteron.

Appendix B

Recursive algorithm and adaptive control

B.1 Simulink scheme for the hysteresis identification

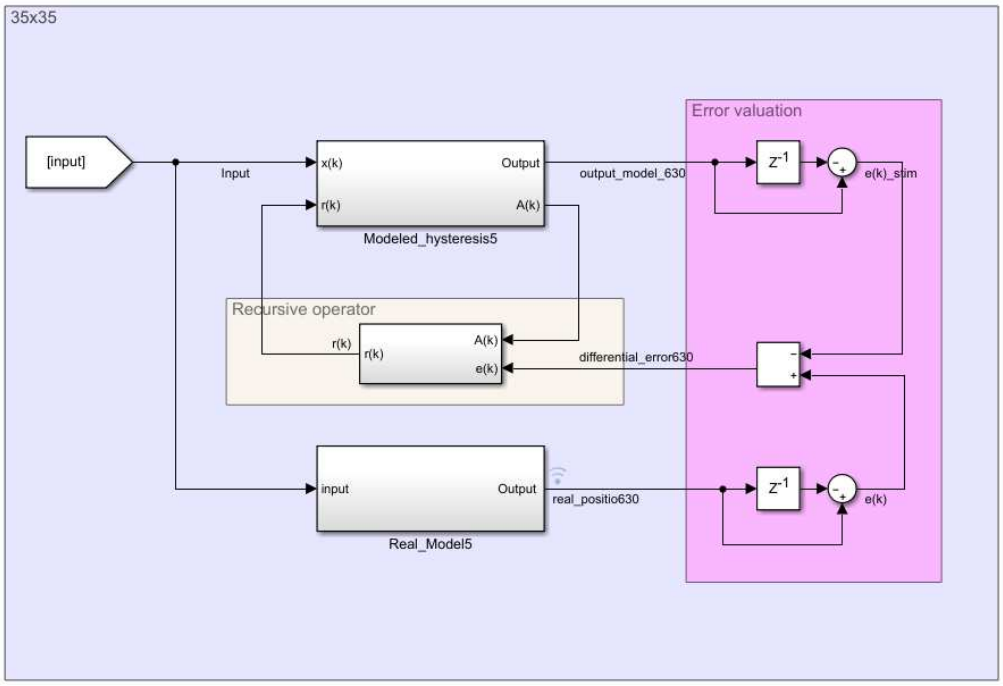

Figure B.1: Simulink scheme of the hysteresis identification model.

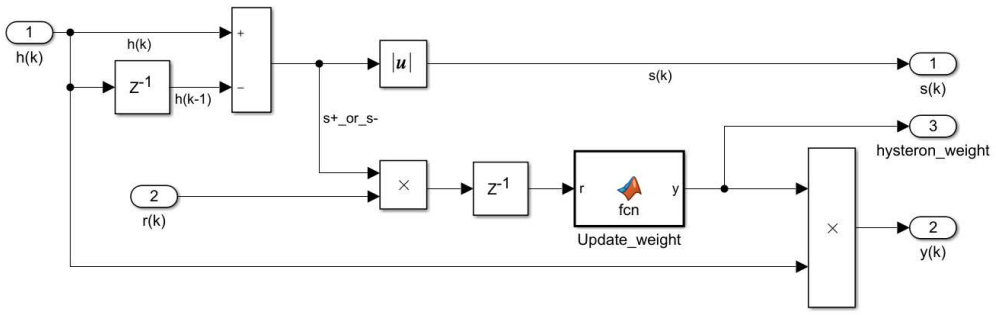

Figure B.2: Simulink scheme of the switching identification and weight correction of a single hysterons.

B.2 Matlab script for the hysteresis representation of the actuator hysteresis

```
function output  = hyst(input)

% Declaration and initialization of the
   variables
persistent old_output;
persistent old_input;
persistent old_cond;
persistent old_slope;

if isempty(old_output)
old_output = 0;
end

if isempty(old_input)
old_input = 0;
end

if isempty(old_cond)
old_cond = 0;
end

if isempty(old_slope)
old_slope = 0;
end

```

```
25          slope = 0;      % if input is increasing slope
               = 1; if input is decreasing slope = 0
26          cond = 0;       % determine in what section of
               the hysteresis shape the ipnut belongs
27          output = 0;
28          first = 0;      % statement that indicate if
               there has been a change in the input trend
29
30          % Input thresholds
31          % increasing
32          theshold1 = 2.1;
33          theshold2 = 2.16;
34          theshold3 = 3.45;
35          theshold4 = 3.5;
36          theshold5 = 4.68;
37          theshold6 = 4.77;
38
39          % decreasing
40          theshold7 = 3.18;
41          theshold8 = 3.13;
42          theshold9 = 1.8;
43          theshold10 = 1.74;
44          theshold11 = 0.55;
45          theshold12 = 0.5;
46
47          % Output levels
48          % increasing
49          level1 = 6.8e-5;
50          level2 = 1.42e-4;
51          level3 = 2.2e-4;
52
53          % decreasing
54          level4 = 1.44e-4;
55          level5 = 7e-5;
56
57          % Slopes
58          % increasing
59          m1 = (level1)/(theshold2 - theshold1);
60          m2 = (level2 - level1) / (theshold4 - theshold3
               );
61          m3 = (level3 - level2) / (theshold6 - theshold5
               );
62
```

```
63          % decreasing
64          m4 = (level3 - level4) / (theshold7 - theshold8
               );
65          m5 = (level4 - level5) / (theshold9 -
               theshold10);
66          m6 = (level5) / (theshold11 - theshold12);
67
68          % Increasing input behaviour
69
70          if input-old_input > 0
71          slope = 1;
72
73          % Condition identification
74          if input >= 0
75          cond = 0;
76          end
77          if input >= theshold1
78          cond = 1;
79          end
80          if input >= theshold2
81          cond = 2;
82          end
83          if input >= theshold3
84          cond = 3;
85          end
86          if input >= theshold4
87          cond = 4;
88          end
89          if input >= theshold5
90          cond = 5;
91          end
92          if input >= theshold6
93          cond = 6;
94          end
95
96          % Considerations:
97          % - if condition is even then the output is
               constant;
98          % - if condition is odd the output is
               propotional to input.
99
100         % Unchanged condition
101         if cond - old_cond == 0
```

```
102
103         % Condition is even
104         if mod(cond,2) == 0
105         output = old_output;
106         else
107
108         % Condition is odd
109         if cond == 1
110         output = m1 * (input - theshold1);
111         end
112         if cond == 3
113         output = m2 * (input - theshold3) + level1;
114         end
115         if cond == 5
116         output = m3 * (input - theshold5) + level2;
117         end
118         end
119
120         % Changed condition
121         else
122         if input >= 0
123         output = 0;
124         end
125         if input >= theshold1
126         output = m1*(input - theshold1);
127         end
128         if input >= theshold2
129         output = level1;
130         end
131         if input >= theshold3
132         output = m2*(input - theshold3) + level1;
133         end
134         if input >= theshold4
135         output = level2;
136         end
137         if input >= theshold5
138         output = m3*(input - theshold5) + level2;
139         end
140         if input >= theshold6
141         output = level3;
142         end
143         end
144
```

```
145         % Allow orizzontal path for internal loops
146         % Change in the direction of input doesn't
               produce a
147         % jump to the other side of the shape
148         if output - old_output < 0
149         output = old_output;
150         end
151
152         % Decreasing input
153         else
154         slope = 0;
155
156         % Condition identification
157         if input <= 5
158         cond = 6;
159         end
160         if input <= theshold7
161         cond = 7;
162         end
163         if input <= theshold8
164         cond = 8;
165         end
166         if input <= theshold9
167         cond = 9;
168         end
169         if input <= theshold10
170         cond = 10;
171         end
172         if input <= theshold11
173         cond = 11;
174         end
175         if input <= theshold12
176         cond = 0;
177         end
178
179         % If there has been a change in the input trend
               the output % should be egual to the
               previous one until the input     % reaches
               the new decreasing threshold
180         if slope - old_slope ~= 0
181         first = 1;
182         end
183         if first
```

```
184         output = old_output;
185         first = 0;
186         else
187
188         % Unchanged condition
189         if cond - old_cond == 0
190
191         % Input belongs to a 'flat' part of the
               hysteresis
192         if mod(cond,2) == 0
193         output = old_output;
194         else
195
196         % Output decreases with the input
197         if cond == 7
198         output = m4*(input - theshold8) + level4;
199         end
200         if cond == 9
201         output = m5*(input - theshold10) + level5;
202         end
203         if cond == 11
204         output = m6*(input - theshold12);
205         end
206         end
207         else
208
209         % In case of condition variation
210         if input <= 5
211         output = level3;
212         end
213         if input <= theshold7
214         output = m4*(input - theshold8) + level4;
215         end
216         if input <= theshold8
217         output = level4;
218         end
219         if input <= theshold9
220         output = m5*(input - theshold10) + level5;
221         end
222         if input <= theshold10
223         output = level5;
224         end
225         if input <= theshold11
```

```
226         output = m6*(input - theshold12);
227         end
228         if input <= theshold12
229         output = 0;
230         end
231         end
232         end
233
234         % Internal loop managing
235         if output - old_output > 0
236         output = old_output;
237         end
238         end
239
240         old_input = input;
241         old_output = output;
242         old_cond = cond;
243         old_slope = slope;
244
245         end
```

B.3 Simulink scheme for the adaptive algorithm

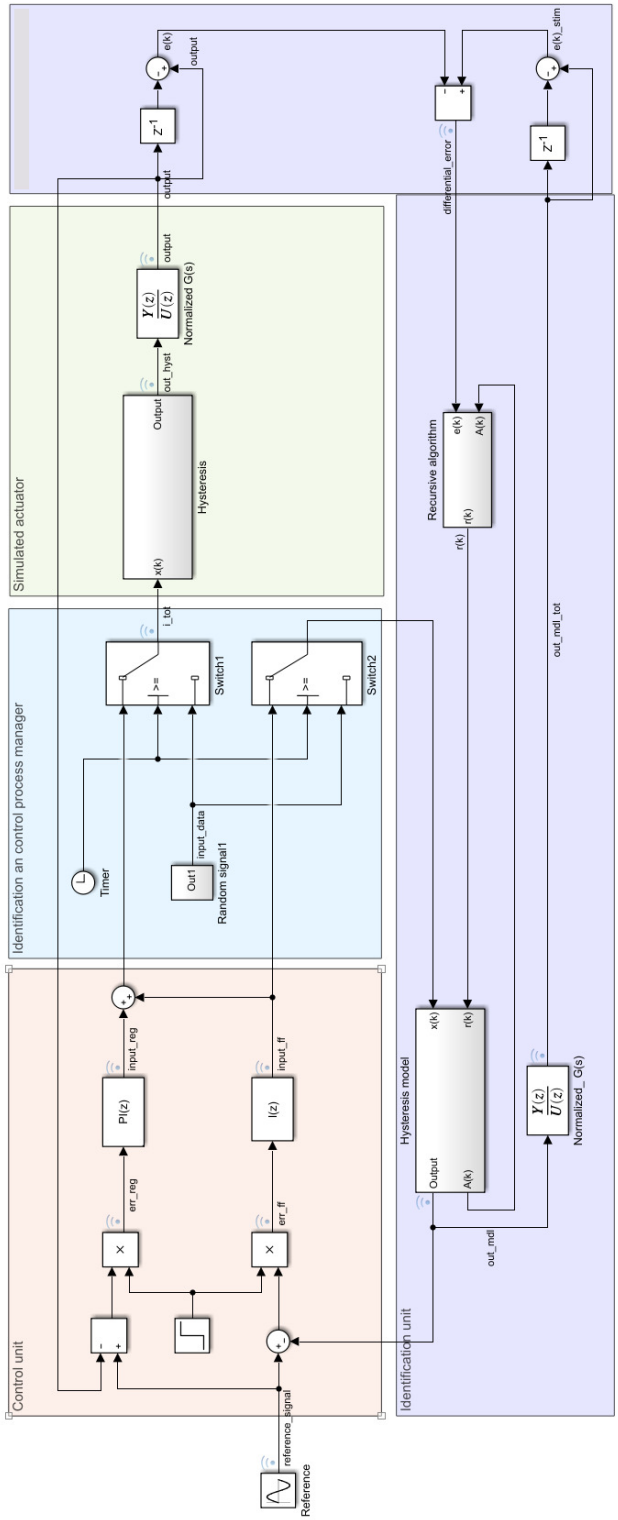

Figure B.3: Simulink scheme of the complete adaptive algorithm.

Appendix C

Tuning and experimental control system

C.1 Simulink scheme for the tuning of the feedforward

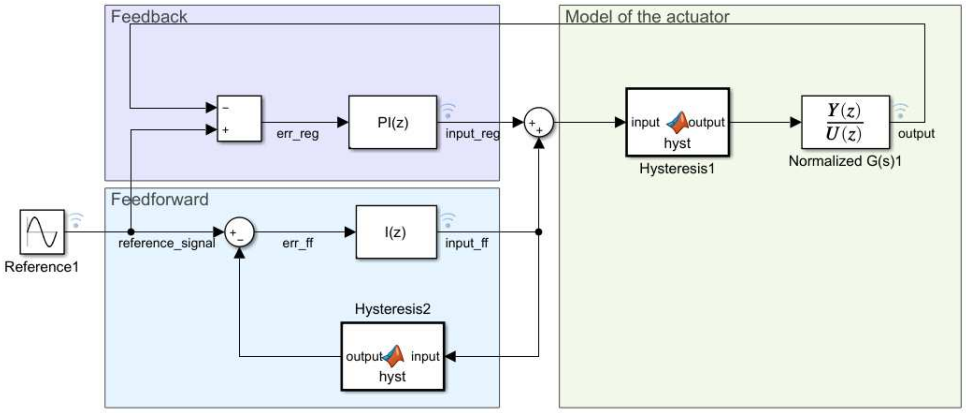

Figure C.1: Simulink scheme for the tuning of the hysteresis compensator.

C.2 Simulink scheme for experimental tests

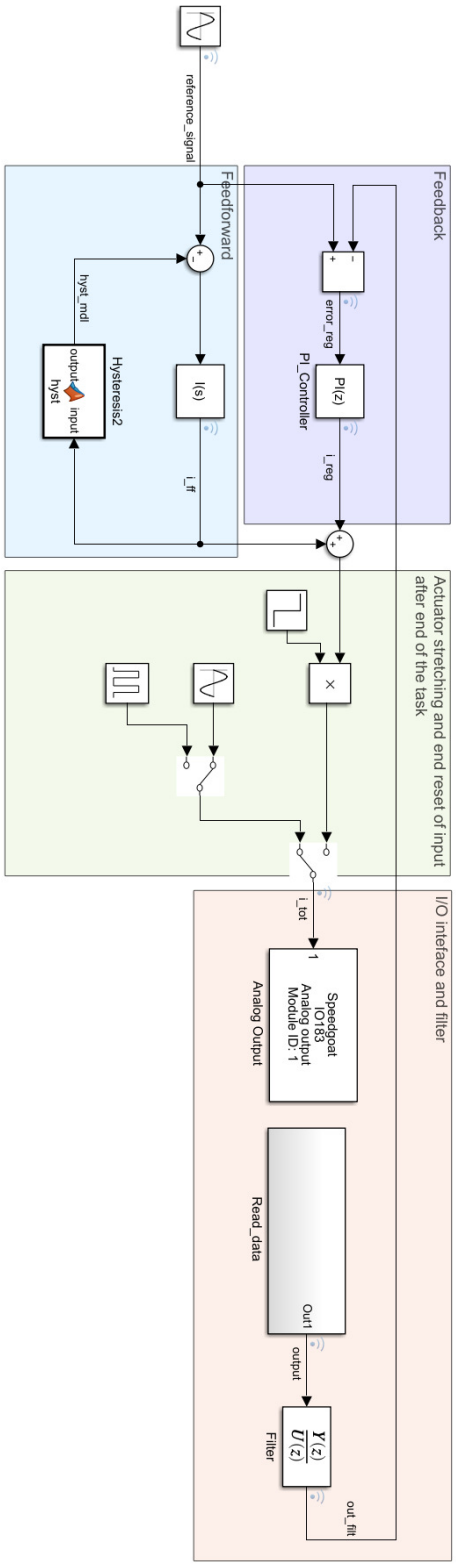

Figure C.2: Simulink scheme for the real-time experimental tests.